Marine Micropaleontology 167 (2021) 102000

Contents lists available at ScienceDirect

Marine Micropaleontology

journal homepage: www.elsevier.com/locate/marmicro

Research paper

Distribution of organic-walled dinoflagellate cysts in surface sediments of the southern Caribbean and the eastern tropical Pacific and its environmental implications

Valentina Ramírez-Valencia [a,b], Manuel Paez-Reyes [c,d], Jorge Salgado [a,e], Francesca Sangiorgi [f], Andrés Camilo Zúñiga-González [a], Adolfo Amézquita [a], Humberto Ibarra-Ávila [g], Catalina González-Arango [a,*]

[a] Departamento de Ciencias Biológicas, Universidad de los Andes, Carrera 1 N° 18A-12, Bogotá 111711, Colombia
[b] Instituto de Investigaciones en Estratigrafía-IIES, Universidad de Caldas, Manizales, Colombia
[c] Earth and Atmospheric Science Department, University of Houston, Houston, United States
[d] Smithsonian Tropical Research Institute, Balboa-Ancón, 0843-03092 Panamá, Panamá
[e] Facultad de Ingeniería, Universidad Católica de Colombia, Bogotá, Colombia
[f] Dept. Earth Sciences, Marine Palynology and Paleoceanography, Utrecht University, the Netherlands
[g] Centro de Microscopía, Vicerrectoría de Investigaciones, Universidad de los Andes, Bogotá, Colombia

ARTICLE INFO

Keywords:
Eastern tropical Pacific
Dinoflagellates
Biogeography
Southern Caribbean
Upwelling
Plankton ecology

ABSTRACT

Little is known about the marine palynology of the neotropical oceans. Here, we present the first comprehensive study of organic-walled dinoflagellate cyst assemblages in 52 surface marine sediment samples from the southern Caribbean (SC) and the eastern tropical Pacific (ETP) and explain how these assemblages relate to sea-surface parameters. Multivariate analyses show that of the several environmental parameters considered, sea-surface salinity (SSS), phosphate concentrations, and nitrate concentrations best explain the relative abundances and the geographic distribution of dinoflagellate cysts in the studied area. Consistent with regional differences in marine productivity, dinoflagellate cyst concentrations were markedly different in the SC (1979 ± 1053 cysts/g) and the ETP (3105 ± 1956 cysts/g). Sediments of the SC are characterized by high relative abundances of the *Spiniferites* spp. group, cysts of *Protoceratium reticulatum*, and the presence of rare dinocyst taxa. The dinocyst assemblages from the ETP are characterized by higher relative and absolute abundances of *Bitectatodinium spongium, Brigantedinium* spp., and *Echinidinium aculeatum*. This pattern is explained by the more eutrophic nature of the ETP compared to the highly saline and oligotrophic SC. Average values of the Shannon Index (H') from the ETP are higher compared to the SC, demonstrating that dinocysts respond to the greater climatic variability that characterizes the ETP. *Brigantedinium* spp. abundances are negatively correlated to H' diversity supporting its dominant character within the dinocyst community. This work fills a gap in our knowledge on modern dinocyst distribution in neotropical oceans and provides a modern reference for interpreting down core dinocyst variations and paleocenographical reconstructions in the region.

1. Introduction

Dinoflagellates are a group of marine and freshwater planktonic eukaryotic organisms (Taylor et al., 2008). As one of the most important primary producers, dinoflagellates are not only responsible for transferring energy from the base of the trophic food web but also for carbon export to the deep ocean (Müller-Karger et al., 2004; Bravo and Figueroa, 2014; Guidi et al., 2016). Their different feeding strategies that include autotrophy, heterotrophy, and mixotrophy along with their diverse habitats allowed dinoflagellates to thrive in the ocean since the Mesozoic (Schnepf and Elbrächter, 1992; Gaines and Elbraechter, 1987; Dale, 2001; Taylor et al., 2008). Their complex life cycle, which alternates asexual and sexual phases, has further allowed these organisms to successfully endure severe environmental change. Following both sexual (hypnozygote) and asexual reproduction, resting cysts (henceforth referred as dinocyst) can develop (Wall, 1965; Figueroa et al., 2008;

* Corresponding author.
E-mail address: c.gonzalez2579@uniandes.edu.co (C. González-Arango).

https://doi.org/10.1016/j.marmicro.2021.102000
Received 19 June 2020; Received in revised form 6 May 2021; Accepted 10 May 2021
Available online 14 May 2021

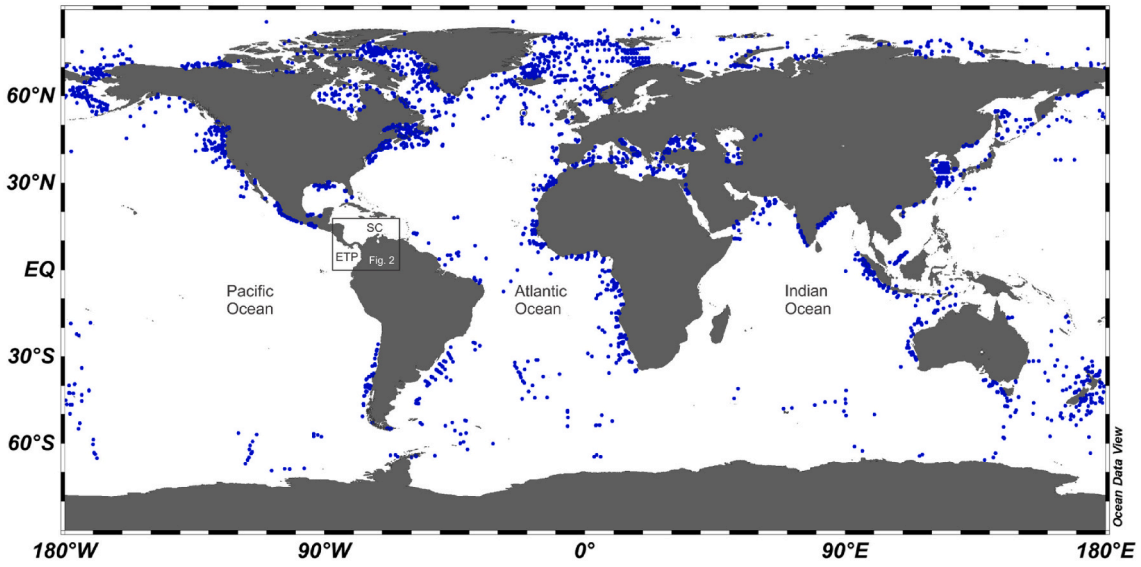

Fig. 1. Geographic location of surface sediment samples included in the dinocyst database of Marret et al., 2020. The black square highlights the study area and the location of the southern Caribbean (SC) and the eastern tropical Pacific (ETP). Map modified from Marret et al. (2020).

Bravo and Figueroa, 2014). About 15–20% of species are capable of producing viable dinocysts that can be preserved in sediments and rocks over long-term temporal scales (Head, 1996).

Dinocysts have provided paleontologists with a valuable tool based on which to interpret and infer evolutionary trajectories (Wall and Dale, 1968; Evitt, 1985) and past ecological and climatic conditions (Dale, 1983; Dale, 2001; de Vernal et al., 1997). Comprehensive research on dinocyst occurrences in surface sediments from the ocean has also provided a wealth of information on their distributions and the main environmental variables driving their occurrences (Harland, 1983; Rochon et al., 1999; Marret and Zonneveld, 2003; Pospelova et al., 2008; Zonneveld et al., 2013; Marret et al., 2020; Van Nieuwenhove et al., 2020). The most critical environmental factors that control the distribution of dinocysts in the modern ocean seem to be sea-surface temperature (SST), sea-surface salinity (SSS), phosphate concentrations ([PO_4]), nitrate concentrations ([NO_3]), water depth (WD), and distance to the coast (DC) (Wall et al., 1977; Marret and Zonneveld, 2003; Zonneveld et al., 2013).

The diversity and abundance of dinocysts is seemingly higher in temperate and tropical latitudes, but endemic polar and sub-polar dinocyst species have also been recorded (Mudie, 1992; Montresor et al., 2003; Limoges et al., 2018; Marret et al., 2020). Despite this, the majority of studies on dinocyst morphology and ecology have focused on the northern temperate and high latitudes (de Vernal et al., 1997, 2001, 2020; Rochon et al., 1999; Orlova et al., 2004; Marret et al., 2001; Esper and Zonneveld, 2002; Matthiessen et al., 2005; Crouch et al., 2010; Prebble et al., 2013; Zonneveld et al., 2013; Price et al., 2016; Mudie et al., 2017; Allan et al., 2020; Marret et al., 2020) (Fig. 1, blue dots), whereas dinocyst distribution in tropical areas such as the southern Caribbean Sea and the eastern tropical Pacific Ocean remains

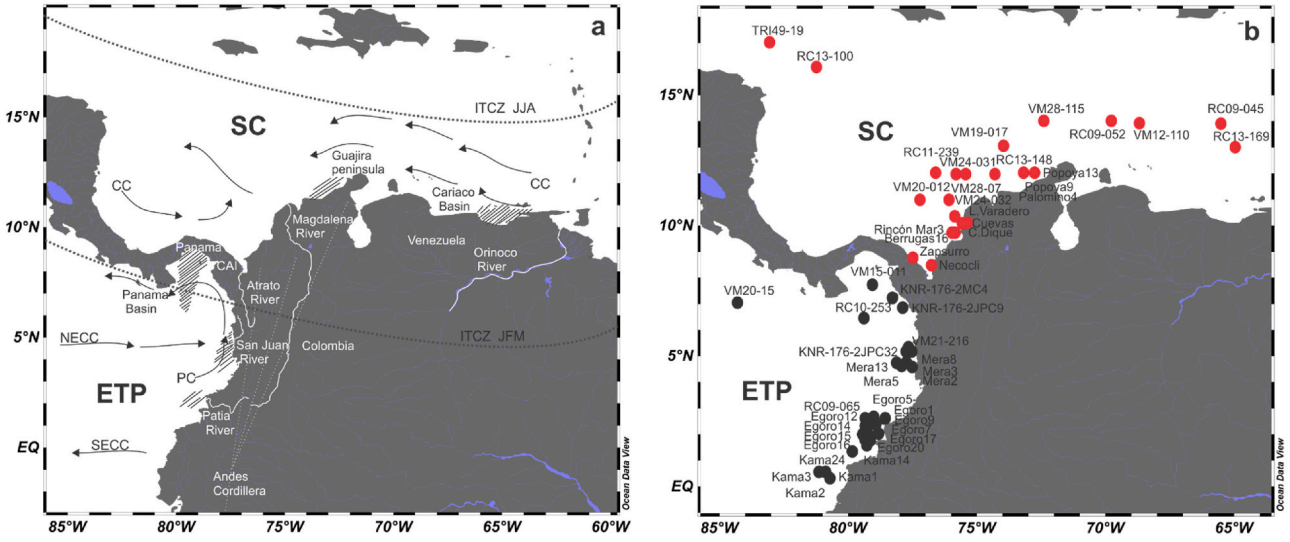

Fig. 2. a- Oceanic currents, upwelling cells, Intertropical Convergence Zone (ITCZ) seasonal position, and drainage system in the southern Caribbean (SC) and the eastern tropical Pacific (ETP). Oceanic currents: Caribbean Current (CC), Pacific Current (PC), North Equatorial Counter Current (NECC), South Equatorial Current (SECC). Hatched pattern: Upwelling zones. The dotted lines delimit the position of the ITCZ in June–July–August (JJA) and January–February–March (JFM). Also shown are the Central American isthmus (CAI) and the Andes Cordillera. The relevant rivers for this study are shown in white; note how the Magdalena, Atrato, and Orinoco rivers flow into the SC, and the San Juan and Patia rivers flow into the ETP (Restrepo and Kjerfve, 2004; Poveda et al., 2006, 2014; González et al., 2008). b- Location of studied samples (the red dots show the location of samples from the SC and the black dots the location of samples from the ETP).

Table 1
Locality (light typeface = southern Caribbean (SC), bold typeface = eastern tropical Pacific (ETP)); longitude (Long); latitude (Lat); sea-surface temperature (SST) in °C, Annual: SST_A; June–July–August: SST_JJA; January–February–March: SST_JFM; sea-surface salinity (SSS) in psu, Annual: SSS_A; June–July –August: SSS_JJA; January–February–March: SSS_JFM; the sea-surface concentration of phosphates [PO4] in μmol/L, Annual: [PO4]_A; June–July–August: [PO4]_JJA; January–February–March: [PO4]_JFM; the sea-surface concentration of nitrates [NO3] in μmol/L, Annual: [NO3]_A; June–July–August: [NO3]_JJA; January–February–March: [NO3]_JFM. Water depth in m (WD); Distance to the coast in m (DC). All SSTs, SSSs, and nutrient concentrations were downloaded from the World Ocean Atlas (Boyer et al., 2013). Repositories (R): Laboratorio de Biología Molecular Marina (BIO); Universidad EAFIT (EAF); Lamont–Doherty Earth Observatory (LDE); Laboratorio de Palinología y Paleoecología tropical (PPT); Ocean Drilling Program (ODP), Instituto Colombiano del Petróleo (ICP). Device: Sampling method/tool.

Locality	Long	Lat	SST_A	SST_JJA	SST_JFM	SSS_A	SSS_JJA	SSS_JFM	[PO4] _A	[P] O4_ JJA	[P O4] _ JFM	[NO3] _A	[NO3] _JJA	[NO3] _ JFM	WD	DC	R	Device
CUEVAS	−75.6	10	28.69	28.7	27.2	34.37	35.7	36.8	0.02	0.01	0.47	0.1	0	0	4	2	BIO	
L.VARADERO	−75.6	10	28.69	28.7	27.2	34.37	35.7	36.8	0.02	0.01	0.47	0.1	0	0	4	2	BIO	Diving
RC13–100	−81.2	16	28.11	27.7	26.7	36.14	36.2	36.1	0.042	0.03	0.05	0.96	0	0	4570	244.9	EAF	Piston Core
VM28–115	−72.4	14	28.29	27.3	26.4	32.18	35.9	35.7	0.056	0.26	0.06	0.3	4.578	0	2109	178	LDE	Piston Core
TRI 49–19 I	−83	17	28.11	28	26.1	36.04	36.1	35.9	0.04	0.03	0.05	1.21	0	0	1830	177.5	EAF	Piston Core
NECOCLÍ	−76.8	8.4	28.5	28.9	27	33.69	36.2	36.8	0.01	0.01	0.47	0.1	0.1	3.4	15	1.56	PPT	Diving
ZAPSURRO	−77.5	8.8	27.27	28.9	27	35.66	36.2	36.8	0.014	0.01	0.47	0.13	0	3.4	30	8.63	PPT	Diving
RC13–169	−65	13	27.51	28.3	26	35.72	36.5	35.8	0.065	0.06	0.03	0.49	2.2	0.867	4649	177.5	LDE	Piston Core
VM12–110	−68.7	14	27.52	27.7	26.3	35.72	35	35.7	0.108	0.03	0.24	0.61	4.578	0	5040	159.6	LDE	Piston Core
RC09–052	−69.8	14	27.41	27.4	26.2	35.72	36.5	35.9	0.081	0.03	0.105	0	4.578	0	4599	174.9	LDE	Piston Core
VM20–012	−77.2	11	27.86	27.3	26.3	35.92	36.2	35.1	0.027	0	0.05	0.1	4.578	0	3396	177	LDE	Piston Core
RC11–239	−75.5	12	27.23	27.4	26.2	35.62	36.7	36.3	0.032	0.01	0.05	0	4.578	0	3301	122.3	LDE	Piston Core
PALOMINO4	−73.6	11	26.4	26.9	25.5	36.62	36.3	37.1	0.015	0.01	0.05	0.71	4.578	0	25	12.05	PPT	Dredging
POPOYA13	−72.8	12	27.25	25.7	23.8	35.98	36.3	36.5	0.112	0.01	0.05	0.27	4.578	0	1	24.95	PPT	Dredging
VM28–07	−75.8	12	27.08	27.7	26.2	35.9	36.3	36.3	0.01	0.01	0.05	0	4.578	0	2869	99.21	ODP	Piston Core
RC09–045	−65.5	14	27.5	28.3	26.2	35.72	35	35.9	0.037	0.075	0.02	0	0	0	4674	436.4	LDE	Piston Core
VM24–031	−76.6	12	27.56	27.7	26.2	36.29	36.2	36.3	0.06	0	0.05	0.1	4.578	0	3623	218.6	LDE	Piston Core
VM24–032	−76.1	11	28.06	27.8	26.9	35.97	36.3	36.8	0	0	0.05	0.1	0	0	2704	94.8	LDE	Piston Core
VM19–017	−74	13	27.52	26.5	25.1	35.92	36.3	36.7	0.026	0.01	0.05	0.03	4.578	0	3872	151.8	LDE	Piston Core
POPOYA9	−73.1	12	28.62	25.7	23.8	36.02	36.3	37.1	0.015	0.01	0.05	0.71	4.578	0	1	17.13	PPT	Dredging
RINCÓN MAR3	−75.8	9.8	28.86	28.8	27.2	34.31	35.7	36.8	0.01	0.01	0.47	0.1	0	0	36	2.61	PPT	Dredging
RC13–148	−74.3	12	27.08	26.9	25.5	35.7	36.3	37.1	0.015	0.01	0.05	0.71	4.578	0	1257	45.07	LDE	Piston Core
C.DIQUE	−75.5	10	29.2	28.7	27.2	34.37	35.7	36.8	0.02	0.01	0.47	0.1	0	0	4	2	BIO	Diving
BERRUGAS16	−76	9.7	28.86	28.8	27.2	34.31	35.7	36.8	0.01	0.01	0.47	0.1	0	0	26	20.04	PPT	Dredging
EGORO1	−78.6	2.5	26.75	26.8	26.2	29.99	32.9	31.8	0.382	0.35	0.15	1.89	0	0.1	76	6.47	ICP	Piston Core
EGORO5	−79	2.5	26.77	26.8	26.2	32.36	32.9	31.8	0.382	0.35	0.15	3.85	0	0.1	210	47.17	ICP	Piston Core
EGORO7	−78.9	2.3	26.47	26.8	26.2	32.36	32.9	31.8	0.382	0.35	0.15	3.85	0	0.1	768	18.23	ICP	Piston Core
EGORO12	−79.3	2.2	26	26.8	26.2	32.71	32.9	31.8	0.382	0.35	0.15	1.89	0	0.1	591	60.97	ICP	Piston Core
EGORO15	−79.3	1.7	26.47	26.6	26	32.71	32.1	32.2	0.382	0.35	0.215	1.89	0	0.13	839	33.69	ICP	Piston Core
EGORO14	−79.3	1.9	26.47	26.6	26	32.71	32.1	32.2	0.382	0.35	0.215	1.89	0	0.13	797	38.5	ICP	Piston Core
EGORO16	−79.2	1.9	26.23	26.6	26	32.39	32.1	32.2	0.382	0.35	0.215	1.89	0	0.13	686	39.34	ICP	Piston Core
EGORO17	−79.1	1.7	26.47	26.8	26.2	32.71	32.9	31.8	0.382	0.35	0.15	1.89	0	0.1	572	2.77	ICP	Piston Core
EGORO9	−79	2.3	26.47	26.8	26.2	29.42	32.1	31.8	0.382	0.35	0.15	1.89	0	0.1	653	32.53	ICP	Piston Core
EGORO20	−78.8	2	26.47	26.4	27	32.36	32.3	31.1	0.382	0.185	0.125	3.85	0	0.1	664	8.5	ICP	Piston Core
MERA2	−77.5	4.6	28.1	27.8	26.1	26.65	32.3	30.3	0.355	0.185	0.125	1.16	0	0.1	94	15.97	ICP	Piston Core
MERA3	−77.5	5.1	28.1	26.4	27	26.65	32.3	31.1	0.355	0.185	0.125	1.16	0	0.1	66	9.16	ICP	Piston Core
MERA5	−77.9	4.6	26.6	26.4	27	29.99	32.3	31.1	0.355	0.185	0.125	1.16	0	0.1	1534	61.4	ICP	Piston Core
MERA8	−77.7	4.8	26.97	27.8	26.1	27.6	32.3	30.3	0.24	0.185	0.125	6.03	0	0.1	1519	33.12	ICP	Piston Core
MERA13	−77.5	5.2	28.69	27.8	27	28.23	32.6	32.3	0.24	0.45	0.22	6.03	0	0.5	66	9.36	ICP	Piston Core
VM20–015	−84.3	7	27.63	28.1	25.8	32.77	31.3	32.7	0.16	0.19	0.47	0.5	0	3.4	1736	191.2	LDE	Piston Core
VM15–011	−79.1	7.8	26.05	27.5	25.6	33.22	32.5	32.1	0.23	0.185	0.405	0.41	0	6	249	74.42	LDE	Piston Core
RC10–253	−79.4	6.5	27.59	26.8	26.2	32.06	32.9	31.8	0.303	0.35	0.15	0.93	0	0.1	3219	202.9	LDE	Piston Core
RC9–065	−79.3	2.5	26.45	27.8	26.1	32.36	32.3	30.3	0.382	0.185	0.125	1.89	0	0.1	2074	70.03	LDE	Piston Core
VM21–216	−77.6	5.3	27.4	26	25.4	28.39	33.5	33.4	0.24	0.66	0.57	6.03	0.2	5.7	761	22.8	LDE	Piston Core
KAMA3	−81	0.5	25.84	26.1	26	33.17	32.1	32.2	0.236	0.35	0.193	0	0	0.13	3797	106	EAF	Piston Core
KAMA14	−79.2	1.6	26.39	26.6	26.4	32.64	32.8	32.6	0.313	0.35	0.215	3.85	0.2	0.15	784	24.93	EAF	Piston Core
KAMA24	−79.9	1.4	26.27	26	26.9	34.57	33.3	32.7	0.313	0.66	0.57	3.85	0	5.7	1623	47.2	EAF	Piston Core
KAMA1	−80.7	0.3	25.7	26	26.9	33.36	33.3	32.7	0.375	0.66	0.57	0	0	5.7	3046	74.79	EAF	Piston Core
KAMA2	−80.8	0.5	25.97	27.4	26.5	26.65	32.5	31.7	0.375	0.2	0.47	0	0	0.3	1315	78	EAF	Piston Core
KNR176–2 JPC9	−77.9	6.8	26.92	26.4	27	27.02	32.3	31.1	0.268	0.185	0.125	1.15	0	0.1	288	20.92	LDE	Piston Core
KNR176–2-JPC32	−78	4.7	23.17	27.5	26.6	30.74	32.5	31.7	0.355	0.112	0.47	1.16	0	3.4	2195	68.21	LDE	Piston Core
KNR176–2-MC4	−78.2	7.3	28.65	28.5	27.8	30.22	32.3	31.9	0.162	0.45	0.39	0.24	6	3.2	2121	25.09	LDE	Piston Core

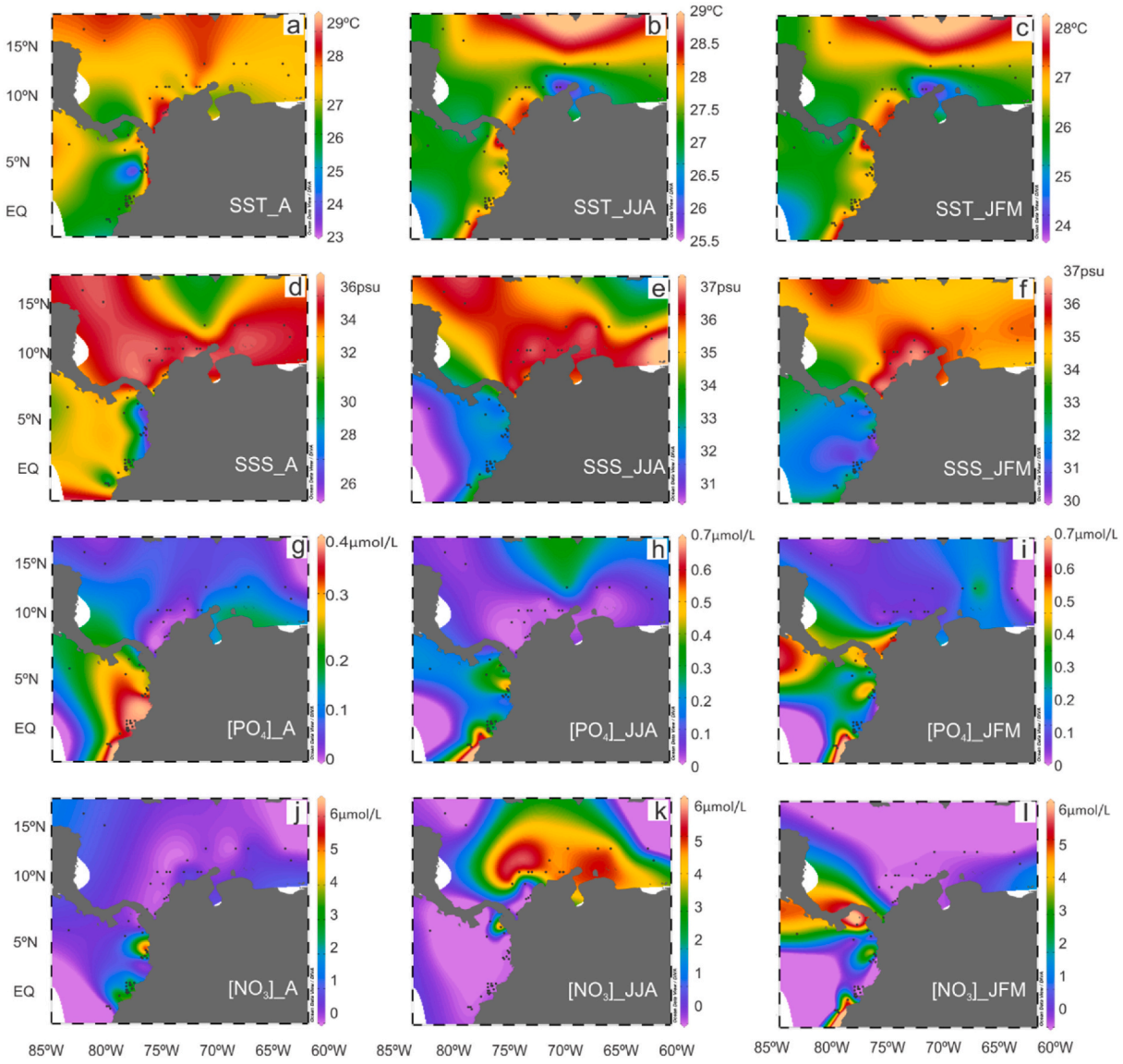

Fig. 3. Surface-water conditions in the southern Caribbean (SC) and the eastern tropical Pacific (ETP). Sea-surface temperature (SST) in °C: a- Annual (SST_A), b- June–July–August (SST_JJA), c- January–February–March (SST_JFM). Sea-surface salinity (SSS) in psu: d- Annual (SSS_A), e- June–July –August (SSS_JJA), f- January–February–March (SSS_JFM). The sea-surface concentration of phosphates ([PO4]) in µmol/L: g- Annual ([PO4]_A), h- June–July–August ([PO4]_JJA), i- January–February–March ([PO4]_JFM). The sea-surface concentration of nitrates ([NO3]) in µmol/L: j- Annual ([NO3]_A), k- June–July–August ([NO3]_JJA), l- January–February–March ([NO3]_JFM). Values were downloaded from the World Ocean Atlas 2013 (Boyer et al., 2013).

underexplored (Fig. 1, black square). While the range of climatic variability in these areas is smaller than that which is observed in temperate and high latitudes (Boyer et al., 2013), the few studies available suggest that the composition and distribution of dinocysts vary in space and time, in response to some of the above-mentioned environmental parameters (Wall et al., 1977; Lewis et al., 1990; Vink et al., 2000; Vásquez-Bedoya et al., 2008; González et al., 2008; Limoges et al., 2010, 2013; Bringué et al., 2019).

The purpose of this study was to examine the spatial distribution of dinocysts in marine surface sediments from the southern Caribbean (SC) and the eastern tropical Pacific (ETP) in order to: 1) document the dinoflagellate assemblages on a regional scale; 2) assess the main environmental parameters that drive the distribution of dinocysts and how these variables shape the abundance and diversity in both areas; and 3) set a modern baseline for dinocyst assemblages based on which paleoenvironmental reconstructions can be assessed.

2. Oceanography of the southern Caribbean (SC) and eastern tropical Pacific (ETP) areas

The study area is located between latitudes 0° N to16° N and longitudes 65° W to 84° W (Fig. 2). The modern oceanography of the SC and ETP is the result of a complex geologic history in which the collision between the western margin of the South American Plate and the Caribbean Plate gave rise 13–4 Ma to the Central American Isthmus (CAI) and Colombia's eastern Cordillera (Fig. 2a) (Mora et al., 2006; Montes et al., 2015; O'Dea et al., 2016). This geological process brought a long-established connection between the SC and the ETP to an end, and, in turn, changed the hydrographic and atmospheric conditions in these basins (O'Dea et al., 2016). The closure of the CAI caused a major reorganization of the ocean circulation. As a result, the waters of the Caribbean became highly saline (36 psu) and over saturated in $CaCO_3$, contrasting with the low saline (33 psu) and more corrosive waters characteristic of the Pacific (Haug and Tiedemann, 1998). Also, the SC is characterized by lower mean primary-productivity values (71–141 g C

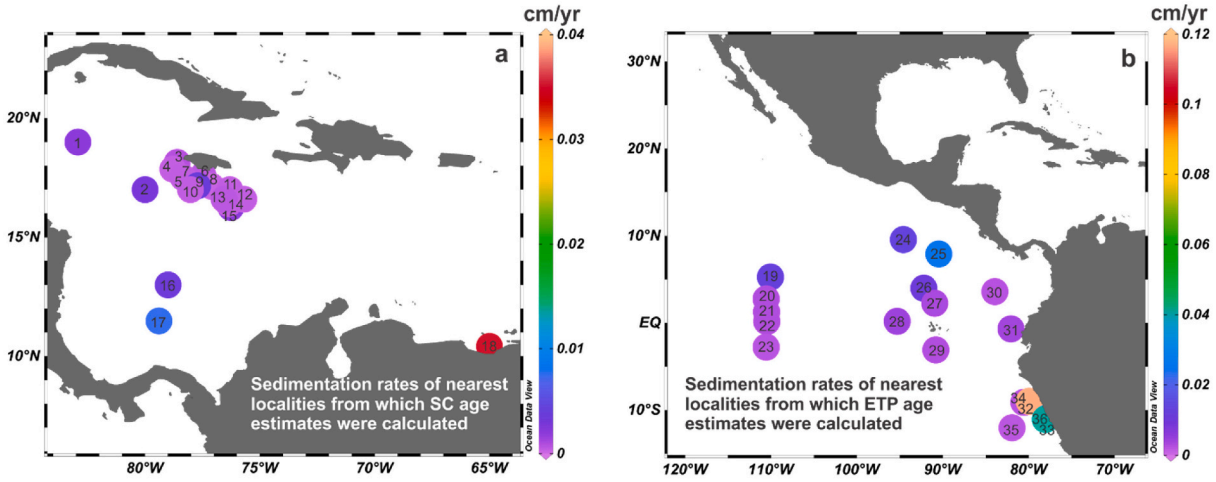

Fig. 4. Distribution maps of sedimentation rates (cm/yr.) used for the age estimation of samples in a- the southern Caribbean (SC), b- the eastern tropical Pacific (ETP).

m^{-2} y^{-1}) than the mean value of 120–363 g C m^{-2} y^{-1} estimated for the ETP (Longhurst et al., 1995; Boyer et al., 2013). The hydroclimatology of the SC and ETP is dominated by seasonal latitudinal shifts of the Intertropical Convergence Zone (ITCZ) from its northernmost position in the months of June–July–August (JJA) to its southernmost position in the months of January–February–March (JFM) (Fig. 2a).

2.1. The southern Caribbean (SC)

The SC is located in the western margin of the Atlantic Ocean on the continental platforms of Panama, Colombia, Nicaragua, and Venezuela (Fig. 2a). In general, nutrient-depleted surface waters characterize the Caribbean Sea except for areas adjacent to river mouths and local upwelling zones (Longhurst et al., 1995; Boyer et al., 2013).

The primary oceanic current in the SC is the Caribbean Current (CC) (Fig. 2a) that feeds the Gulf Current, a surficial current that in turn regulates the global climate by transporting warm, humid and saline waters to the North Atlantic (Haug and Tiedemann, 1998).

In the SC (Fig. 2a), the Magdalena, Atrato, and Orinoco rivers discharge 666 t km^{-2} yr^{-1} of sediments and approximately 47,574 m^3 s^{-1} of freshwater into their adjacent coastal areas (Hernandez-Guerra and Joyce, 2000; Restrepo and Kjerfve, 2004; Restrepo and López, 2008; Mora et al., 2020). In addition to river discharge, another mechanism that explains the localized high levels of primary productivity in the SC consists in the trade winds that impinge on the coastal areas of the Cariaco Basin and the Guajira Peninsula from January to March allowing nutrient-rich cold waters to upwell (Milliman, 1990; Müller-Karger et al., 2004).

The rainy season in SC begins during the late boreal summer when the ITCZ is directly over the southern Caribbean (Fig. 2a; Hu et al., 2004; Müller-Karger et al., 2004). A permanent Caribbean low-level jet, which enhances evaporation and carries humidity across Central America is, to some extent, responsible for a greater salinity in the SC compared to the ETP (Wang, 2007; Poveda et al., 2014).

2.2. The Eastern Tropical Pacific (ETP)

The ETP is located at the eastern end of the equatorial Pacific Ocean, off northwestern South America, on the Panama Basin (Fig. 2a). The western margin and the central part of the ETP is an area of high primary productivity with high nutrient levels (Restrepo and López, 2008; Cabarcos et al., 2014).

The main oceanic currents in the ETP are the Pacific Current (PC), North Equatorial Counter Current (NECC), and South Equatorial Current (SECC) (Fig. 2a). The current system of the ETP is influenced by the Peru–Chile Current System and represents the main route for the exchange of nutrients from high to low latitudes in the South Pacific (Cabarcos et al., 2014).

The ETP is characterized by having river discharges greater than 4709 m^3 s^{-1} that deliver an excess of nutrients into the ocean, hence enhancing primary productivity (Poveda et al., 2006, 2014; Restrepo and López, 2008; Hidalgo et al., 2015). The San Juan River and the Patia River are the main Colombian rivers feeding the ETP (Fig. 2a). Despite these rivers being much shorter, the San Juan and Patia rivers deliver ~8 times the amount of water delivered into the ocean by the rivers that drain into the SC (Restrepo and Kjerfve, 2004). Similarly, the estimated sediment load that drains into the Pacific Ocean from Colombia is ca. 1260 t km^{-2} yr^{-1} (Restrepo and Kjerfve, 2004).

Trade winds drive the surface oceanic currents that include the North Equatorial Counter Current (NECC), the South Equatorial Currents (SEC), and the Pacific current (PC) (Fig. 2a; Fiedler and Talley, 2006).

The Colombian Pacific coast experiences an annual average precipitation of 12,500 mm/year that helps to maintain the ETP's low salinity compared to the SC (Poveda and Mesa, 1997; Restrepo and López, 2008; Durán-Quesada et al., 2012; Boyer et al., 2013).

3. Material and methods

3.1. Sediment samples

Samples were collected over the 1958–2014 period. Twenty-four core-top samples (~0–1 cm) from the SC and twenty-eight core–top samples (~0–1 cm) from the ETP were studied. The samples represent a gradient of coastal (neritic) to oceanic (pelagic) depths on the continental margins and abyssal plain of northwestern South America (Fig. 2b). Details of the geographic location, distance to the coast, water depth, and sampling devices are provided in Table 1.

3.2. Oceanographic parameters

Annual and seasonal sea-surface temperature (SST), sea-surface salinity (SSS), and values of concentrations of sea-surface phosphates [PO_4] and nitrates [NO_3] were downloaded from the World Ocean Atlas and averaged through the 1954 to 2013 period at a resolution of 0.25 degrees (Boyer et al., 2013). A shapefile that contained the values for the environmental parameters was then loaded into QGIS (QGIS Development Team, 2014). The yearly and seasonal average values for each environmental variable were extrapolated and plotted on a map using

Table 2
Sedimentation rates (cm/kyr, cm/yr) based on biostratigraphy, magnetostratigraphy, ^{14}C chronology and, chemostratigraphy for the southern Caribbean (SC) and eastern tropical Pacific (ETP). Long: longitude, Lat: latitude, and SR: sedimentary rate (cm/kyr, cm/yr).

Label	Basin	Locality	Long	Lat	SR(cm/kyr)	SR(cm/yr)	Method	Reference
1	SC	998	-82.93	19	1.9	0.0019	Nannoplankton	Kameo and Bralower, 2000
2	SC	1000	−80	17	2.73	0.0027	Nannoplankton	Kameo and Bralower, 2000
3	SC	PC-117	−78.6	18.15	0.7	0.0007	Oxygen isotopes	Sullivan, 1992
4	SC	PC-108	−78.8	17.86	0.26	0.00026	Oxygen isotopes	Sullivan, 1992
5	SC	PC-11	−77.64	17.46	10.2	0.0102	Oxygen isotopes	Sullivan, 1992
6	SC	PC-21	−77.48	17.6	0.48	0.00048	Oxygen isotopes	Sullivan, 1992
7	SC	PC-37	−78.35	17.51	0.31	0.00031	Oxygen isotopes	Sullivan, 1992
8	SC	PC-54	−77.1	17.14	0.129	0.00012	Oxygen isotopes	Sullivan, 1992
9	SC	PC-46	−77.71	17.16	3.68	0.0036	Oxygen isotopes	Sullivan, 1992
10	SC	PC-65	−76.31	17	0.31	0.00031	Oxygen isotopes	Sullivan, 1992
11	SC	PC-72	−76.27	16.25	1.93	0.0019	Oxygen isotopes	Sullivan, 1992
12	SC	V28–119	−75.7	16.6	0.3	0.0003	Oxygen isotopes	Sullivan, 1992
13	SC	PC-89	−78.03	17	0.34	0.00034	Oxygen isotopes	Sullivan, 1992
14	SC	PC-73	−76.37	16.41	0.27	0.00027	Oxygen isotopes	Sullivan, 1992
15	SC	PC-75	−76.56	16.6	0.48	0.00048	Oxygen isotopes	Sullivan, 1992
16	SC	999	−79	13	3.36	0.0033	Nannoplankton	Kameo and Bralower, 2000
17	SC	502	−79.4	11.49	7.5	0.0075	Paleomag	Gardner, 1982
18	SC	1002	−65	10.42	35	0.035	Oxygen isotopes	Peterson et al., 2000
19	ETP	852	−110.07	5.29	1.2	0.012	Magnetostratigraphy/ Nannoplankton	Kemp, 1995
20	ETP	851	−110.57	2.77	2.5	0.0025	Magnetostratigraphy/ Nannoplankton	Kemp, 1995
21	ETP	850	−110.52	1.29	2.5	0.0025	Magnetostratigraphy/ Nannoplankton	Kemp, 1995
22	ETP	849	−110.51	0.18	2.5	0.0025	Magnetostratigraphy/ Nannoplankton	Kemp, 1995
23	ETP	848	−110.47	29.99	5	0.0005	Magnetostratigraphy/ Nannoplankton	Kemp, 1995
24	ETP	845	−94.59	9.58	1.2	0.013	Magnetostratigraphy/ Nannoplankton	Kemp, 1995
25	ETP	844	−90.48	7.92	2.5	0.025	Magnetostratigraphy/ Nannoplankton	Kemp, 1995
26	ETP	TR163–22	−92.23	3.99	10	0.01	Biostratigraphy	Lea et al., 2000
27	ETP	TR163–19	−90.95	2.26	3	0.003	Biostratigraphy	Lea et al., 2000
28	ETP	847	−95.32	0.193	4	0.004	Biostratigraphy	McCartney et al., 1995
29	ETP	1226B	−90.81	−3.09	2.4	0.0024	^{14}C geochronology	http://www-odp.tamu.edu/publications/201_SR/108/108_5.htm
30	ETP	TR163-31	−83.95	3.6	2	0.002	Biostratigraphy	Kienast et al., 2007
31	ETP	1239	−82.08	−0.67	3.5	0.0035	Bioestratigraphy	Rincón-Martínez et al., 2010
32	ETP	1230D	−80.58	−9.11	2	0.002	^{14}C geochronology	http://www-odp.tamu.edu/publications/201_SR/108/108_5.htm
33	ETP	1227B	−79.95	−8.99	116.7	0.1167	^{14}C geochronology	http://www-odp.tamu.edu/publications/201_SR/108/108_t2.htm#1003206
34	ETP	1229E	−77.95	−10.97	32.3	0.0323	^{14}C geochronology	http://www-odp.tamu.edu/publications/201_SR/108/108_t2.htm#1003206
35	ETP	1231C	−81.94	−12.02	1.5	0.0015	^{14}C geochronology	http://www-odp.tamu.edu/publications/201_SR/108/108_5.htm
36	ETP	1228B	−78.07	−11.06	40.4	0.0404	^{14}C geochronology	http://www-odp.tamu.edu/publications/201_SR/108/108_t2.htm#1003206

the freeware program Ocean Data View (Schlitzer, 2017) (Fig. 3, Table 1). Seasonal values of environmental parameters for each locality were plotted for the periods when the ITCZ is at its northernmost and southernmost position in June–July–August (JJA) and January–February–March (JFM), respectively (Figs. 2a, 3). Water depth values and the distances from the coast for each locality were measured and recorded during each oceanographic expedition.

3.3. Palynological analyses

Sediment samples were dried overnight at 60 °C. Between one and two grams of sediment were processed for palynological analyses. Samples were treated with 10% hydrochloric acid (HCl) and 40% cold hydrofluoric acid (HF) to dissolve carbonates and silicates, respectively (de Vernal et al., 1999) and no oxidation was performed. Tablets of *Lycopodium clavatum* (batch number 1031) containing 20,848 ± 691 spores were added during the decalcification process to achieve a quantitative (palynomorphs/g) analysis of the data (Wood et al., 1996). The demineralized and spiked residue was processed in an ultrasonic bath for no longer than 30 s and subsequently sieved through a 10 μm nylon mesh. Aliquots were strewn onto microscope slides and mounted using glycerin jelly. Dinocysts were counted using a Zeiss Imager A.2 optical microscope under 40× and 100× objectives and photographed using an Olympus FV1000 laser scanning confocal microscope with a 60×/1.42 NA oil immersion objective. Generic and specific dinocyst classification followed the taxonomic nomenclature of Williams et al. (2017). Zonneveld and Pospelova (2015) was used as determination key for modern dinocysts. *Brigantedinum cariacoense*, *Brigantedinium simplex*, and other round brown cysts were grouped as *Brigantedinium* spp. when the orientation of the cysts precluded determination at the species level. Most of the species belonging to the genus *Spiniferites* found in the SC and the ETP were assigned to the *Spiniferites ramosus* that has a cosmopolitan distribution. Very few specimens of *S. bentorii* and *S. mirabilis* were found. We grouped all *Spiniferites* species under the category *Spiniferites* spp.

In the case of "*Operculodinium centrocarpum* sensu Wall and Dale

Table 3
Nearest locality from which age estimates were calculated (NLA), estimated age (yr) for top sediments according to the sedimentation rate framework of reference for all studied sites.

Locality	NLA	Estimated age first cm of sediment (yr)
CUEVAS	502	133
L.VARADERO	502	133
RC13–100	998	526
VM28–115	1002	29
TRI 49–19 I	998	526
NECOCLÍ	502	133
ZAPSURRO	502	133
RC13–169	1002	29
VM12–110	1002	29
RC09–052	1002	29
VM20–012	502	133
RC11–239	502	133
PALOMINO4	1002	29
POPOYA13	1002	29
VM28–07	502	133
RC09–045	1002	29
VM24–031	502	133
VM24–032	502	133
VM19–017	1002	29
POPOYA9	1002	29
RINCÓN MAR3	502	133
RC13–148	502	133
C.DIQUE	502	133
BERRUGAS16	502	133
EGORO1	1239	286
EGORO5	1239	286
EGORO7	1239	286
EGORO12	1239	286
EGORO15	1239	286
EGORO14	1239	286
EGORO16	1239	286
EGORO17	1239	286
EGORO9	1239	286
EGORO20	1239	286
MERA2	TTRI163–31	500
MERA3	TTRI163–31	500
MERA5	TTRI163–31	500
MERA8	TTRI163–31	500
MERA13	TTRI163–31	500
VM20–015	844	40
VM15–011	TTRI163–31	500
RC10–253	TTRI163–31	500
RC9–065	TTRI163–31	500
VM21–216	TTRI163–31	500
KAMA3	TTRI163–31	500
KAMA14	TTRI163–31	500
KAMA24	TTRI163–31	500
KAMA1	TTRI163–31	500
KAMA2	TTRI163–31	500
KNR176–2 JPC9	TTRI163–31	500
KNR176–2-JPC32	TTRI163–31	500
KNR176–2-MC4	TTRI163–31	500

(1966)", we follow Paez-Reyes and Head (2013) in that cysts circumscribed by the morphology described by Wall and Dale (1966) are referred to as cysts of *Protoceratium reticulatum*. We justify our choice based on several lines of evidence: 1) Mertens et al. (2018) described the theca-based dinoflagellate species *Pentaplacodinium saltonense*. According to these authors, the cysts produced by *P. saltonense* more closely resemble to the cyst-based species *Operculodinium israelianum* and *Operculodinium psilatum*; 2) given the tabulation similarities between *P. saltonense*, its cysts, and *Operculodinium bahamense*, it is likely that all *Operculodinium* species are (were) produced by a species related to *P. saltonense*; 3) molecular evidence also suggests that the genera *Pentaplacodinium* and *Protoceratium* are not related at the phylogenetic level and that they form two distinctive clades (Mertens et al., 2018; Wang et al., 2019); 4) the cysts of *Protoceratium reticulatum* were initially described to be from the North Sea where cysts of *O. centrocarpum* sensu Wall and Dale occur abundantly (de Vernal et al., 2020), whereas warm-water *O. israelianum*, and *Pentaplacodinium* have not been recorded. All this evidence strongly supports our argument that cysts of *Protoceratium reticulatum* are the same as what is referred to as *O. centrocarpum* sensu Wall and Dale (1966), and that the use of the latter name only generates confusion.

3.4. Age of the sediments in the southern Caribbean and eastern tropical Pacific

The age of the surface sediments (top 0–1 cm) is unknown, as is the case in virtually all dinocyst studies performed over the past forty years. Indeed, when using surface sediments from piston cores (as we did here for 90% of the samples presented), the uppermost sediments could be missing and assuming a present-day age for the core-top samples is not necessarily accurate. We argue, however, that the top sediment represents the last millennium or less. To prove our point, we calculated the sediment accumulation rates and the estimated age of the samples using the sedimentation rates from nearby localities that have biostratigraphy (McCartney et al., 1995; Kameo and Bralower, 2000; Rincón-Martínez et al., 2010; Kemp, 1995), magnetostratigraphy (Kent and Spariosu, 1982), ^{14}C geochronology (ODP samples) or chemostratigraphy (Gardner, 1982; Sullivan, 1992; Peterson et al., 2000; Lea et al., 2000; Kienast et al., 2007) (Fig. 4; Tables 2, 3).

3.5. Assemblage data and statistical analyses

Two different metrics to express palynomorph representation were used throughout this paper: 1) the concentration of palynomorphs (dinocyst, pollen, and spores) per gram of dry sediment (Table 5) (Stockmarr, 1971; Maher Jr, 1981), and 2) the proportion of each dinocyst taxon or group relative to the total dinocyst counts in a given assemblage.

To represent the dinocyst assemblages, we used a diagram of relative abundances by region and a shaded plot. The shaded plot input data corresponded to the square root of dinocyst relative abundances to minimize the effects of dominant species in each sample following Mudie et al. (2017).

We counted the total pollen and spores in the samples as one group. Statistical analyses were performed on fifty-two samples, and the Shannon–Wiener index (H') was used to estimate the diversity and evenness of taxa across space (Table 5). Similar to Marret et al. (2001), we used a minimum of 50 specimens as a cut-off value to include a sample in the statistical analyses. We acknowledge that samples with low counts (less than 100 dinocysts) might underestimate the diversity and artificially over or underrepresent some species in a particular sample (Table 4) and thus bias the diversity index estimation. Nevertheless, a 50 dinocyst cut-off value has proved to represent the main dinocyst species in areas with relative low cyst densities (Marret et al., 2001).

To evaluate environmental heterogeneities within SC and ETP localities, a non-metric multidimensional scaling (NMDS) was applied to the SST, SSS, and $[PO_4]$ and $[NO_3]$ data using the Bray-Curtis index as the comparison metric (Legendre and Gallagher, 2001). To assess for relationships between environmental parameters and dinocyst taxa with abundances higher than 1%, a redundancy analysis was performed (RDA; Legendre and Gallagher, 2001). Cyst raw counts were transformed to Hellinger distances to enable common taxa to be weighted equally to rare species in the statistical analysis (Legendre and Gallagher, 2001). Scaling and transformation of environmental parameters was performed prior to RDA (Legendre and Gallagher, 2001). The relative abundances of the six more dominant dinocyst taxa were overlaid on the environmental NMDS values using bubble plots to show the geographic distribution and relative abundance of these taxa in the multivariate space (Mudie et al., 2017).

Dinocysts were grouped according to nutritional strategies into heterotrophs and autotrophs following Schnepf and Elbrächter (1992)

Table 4

Raw counts of organic-walled dinoflagellate cysts reported from surface samples from the southern Caribbean (SC) and the eastern tropical Pacific (ETP). *Bitectatodinium spongioum*. (BSPO), *Brigantedinium* spp. (BSPP), Cysts of *Archaeperidinium bailongense* (ABAI), Cysts of *Archaeperidinium constrictum* (ACON), Cysts of *Polykrikos schwartzii* (PSCH), cysts of *Protoceratium reticulatum* (PRET), *Echinidinium aculeatum* (EACU), *Echinidinium granulatum* (EGRA), *Echinidinium* spp. (ESPP), *Impagidinium aculeatum* (IACU), *Lingulodinium machaerophorum* (LMAC), *Lejeunecysta* sp. (LESP), *Nematosphaeropsis lemniscata* (NLEM), *Operculodinium israelianum* (OISR), *Selenopemphix nephroides* (SNEP), *Selenopemphix quanta* (SQUA), *Spiniferites* spp. (SSPP), *Stelladinium bifurcatum* (SBIF), *Tuberculodinium vancampoae* (TVAN), *Votadinium spinosum* (VSPI), *Votadinium* sp. (VSPP).

Locality	BSPO	BSPP	ABAI	ACON	PSCH	PRET	EACU	EGRA	ESPP	IACU	LMAC	LESP	NLEM	OISR	SNEP	SQUA	SSPP	SBIF	TVAN	VSPI	VSPP	TOTAL
CUEVAS	1	120	0	0	0	2	0	0	0	0	0	0	0	0	6	0	1	0	0	0	0	130
L.VARADERO	0	38	1	0	0	4	0	1	1	0	0	0	0	0	1	5	1	0	0	1	4	58
RC13–100	148	0	0	1	0	0	0	0	0	0	0	0	0	0	27	0	3	1	0	0	0	180
VM28–115	2	65	0	0	0	7	3	0	0	0	0	0	1	0	0	0	1	0	0	0	0	79
TRI 49–19 I	17	69	0	2	0	6	10	2	0	0	0	0	0	0	4	4	2	0	0	0	0	116
NECOCLÍ	10	71	0	1	0	8	11	0	0	0	0	0	0	0	1	3	2	0	0	0	0	107
ZAPSURRO	10	34	0	0	0	7	2	0	0	1	0	0	0	0	19	0	4	0	0	0	0	77
RC13–169	0	49	0	0	0	1	5	0	0	0	0	0	0	0	1	0	10	1	0	0	0	67
VM12–110	0	0	0	0	0	10	0	0	0	0	0	0	0	0	63	0	0	0	0	0	0	73
RC09–052	0	54	0	0	0	2	0	0	0	0	0	0	0	0	0	0	1	0	0	0	0	57
VM20–012	1	58	0	0	0	1	0	0	0	0	0	0	0	0	2	0	0	0	0	0	0	62
RC11–239	0	46	0	0	0	1	0	0	0	0	1	0	0	0	2	0	0	0	0	0	0	50
PALOMINO4	3	74	0	0	0	10	0	1	0	0	1	0	0	0	2	0	11	0	1	0	0	103
POPOYA13	2	187	0	0	0	1	0	0	0	0	0	0	0	0	4	0	0	0	0	0	0	194
VM28–07	0	38	0	0	0	6	0	0	4	0	0	0	0	0	2	0	0	1	0	0	0	55
RC09–045	0	59	0	0	0	3	0	0	0	0	0	0	0	0	0	0	4	0	0	0	0	66
VM24–031	0	50	0	0	0	0	0	0	0	0	0	0	0	0	8	0	0	0	0	0	0	58
VM24–032	3	66	0	0	0	1	0	0	0	0	0	0	0	0	0	0	0	1	0	0	0	71
VM19–017	0	62	0	0	0	0	0	0	6	0	0	0	0	0	0	0	0	0	0	0	0	74
POPOYA9	0	51	0	0	0	0	4	0	6	0	0	0	0	0	3	0	0	0	0	0	0	70
RINCÓN MAR3	0	44	0	0	0	2	0	1	0	0	0	0	0	0	4	0	3	0	0	0	0	54
RC13–148	0	47	0	0	0	0	0	0	0	1	1	0	0	0	0	0	2	0	0	0	0	51
C.DIQUE	1	32	0	0	0	7	0	0	0	1	1	0	0	1	0	0	14	0	0	0	0	57
BERRUGAS16	0	36	0	0	2	5	2	0	0	0	0	0	5	0	3	0	1	0	0	0	0	54
EGORO1	15	57	3	0	0	2	9	6	1	0	0	0	2	2	1	1	0	0	0	0	1	101
EGORO5	39	104	1	0	2	0	11	4	8	0	0	0	2	0	11	0	6	0	1	0	1	198
EGORO7	17	58	1	0	3	0	19	1	0	0	0	0	0	3	6	0	2	0	1	0	0	111
EGORO12	3	68	1	0	0	0	1	1	0	0	0	0	0	0	4	1	1	0	0	0	0	80
EGORO15	26	96	1	0	1	0	7	2	0	0	1	0	0	0	2	0	0	0	2	0	0	138
EGORO14	4	42	0	0	0	0	4	1	0	0	0	0	1	0	2	0	0	0	0	0	0	54
EGORO16	30	90	0	0	1	0	13	2	0	0	2	0	0	0	2	1	0	0	0	0	1	142
EGORO17	17	91	0	0	2	6	9	5	0	0	1	0	0	4	2	0	0	0	0	1	0	138
EGORO9	57	133	1	1	3	0	8	3	0	0	0	1	0	1	2	0	0	0	0	0	0	210
EGORO20	57	269	2	0	4	2	12	3	2	0	0	0	0	1	2	0	1	0	0	0	2	359
MERA2	16	175	1	0	2	0	8	3	0	0	0	0	0	1	3	0	0	0	0	0	0	209
MERA3	35	120	1	0	2	0	6	5	0	0	1	0	0	2	3	0	0	0	0	0	0	175
MERA5	26	89	0	0	2	1	2	0	0	0	0	0	0	0	0	0	0	0	0	0	0	120
MERA8	10	178	2	0	1	0	2	1	0	0	0	0	0	0	4	1	0	0	0	0	0	199
MERA13	11	63	3	0	2	0	4	5	0	0	0	0	0	0	3	0	1	0	0	0	0	92
VM20–015	12	104	1	0	1	0	8	1	0	0	0	0	0	0	3	0	2	0	0	0	0	132
VM15–011	11	80	1	0	2	2	5	0	0	0	0	0	0	3	6	0	2	0	0	0	0	112
RC10–253	43	91	0	0	1	1	20	0	0	0	1	0	2	0	3	0	5	0	0	0	0	167
RC9–065	38	172	0	0	7	0	21	0	1	0	0	0	1	0	4	0	4	0	1	0	0	250
VM21–216	62	70	0	0	2	0	2	1	0	0	1	0	1	1	0	0	2	0	0	0	0	142
KAMA3	27	72	0	1	1	5	6	1	0	1	0	0	0	0	2	7	2	0	0	1	0	126
KAMA14	27	271	0	0	3	2	23	1	0	0	1	0	1	0	10	3	6	0	0	0	0	348
KAMA24	20	240	0	1	1	15	17	2	1	1	1	0	0	0	9	3	5	0	0	2	0	319
KAMA1	9	90	0	0	5	15	8	0	0	0	0	0	0	1	0	0	2	0	0	0	0	130
KAMA2	28	126	0	0	0	2	16	3	2	2	0	0	1	0	4	1	2	0	0	0	0	189
KNR176–2 JPC9	32	185	0	2	1	3	17	4	0	0	0	0	0	0	4	1	4	0	0	1	0	254
KNR176–2-JPC32	22	168	1	2	1	2	10	1	0	1	0	0	2	0	3	1	10	0	0	0	0	224
KNR176–2-MC4	41	98	0	0	0	0	5	1	0	0	0	0	0	0	0	1	0	0	0	0	0	146

Table 5
Pollen and spores count (p + s count), dinocyst count, *Lycopodium* sp. count (*Lycopodium* count), concentration of pollen and spores per gram of dry sediment (p + s/g), pollen and spores per cm^2 per year (p + s/cm^2/yr), pollen and spores per m^2 per year (p + s/m^2/yr), organic-walled dinoflagellate cyst concentration per gram of dry sediment (dinocysts/g), dinoflagellate cyst per cm^2 per year (dinocysts/cm^2/yr), dinoflagellate cyst per m^2 per year (dinocyst/m^2/yr), Shannon–Wiener index (*H′*) and Heterotrophic/Autotrophic ratio (H/A) for all studied samples.

Locality	p + s count	dinocyst count	Lycopodium count	p + s/g	p + s/cm^2/yr	p + s/m^2/yr	dinocyst/g	dinocyst/cm^2/yr	dinocyst/m^2/yr	H′	H/A
CUEVAS	259	130	1059	4012	2.9	28,554	3253	1.4	14,332	0.35	97
L.VARADERO	312	58	1120	4570	2.3	23,400	1585	0.4	4350	1.21	90
RC13–100	129	180	2705	1565	0.3	3235	3526	0.5	4514	0.76	16
VM28–115	60	79	2140	920	2.6	26,250	1956	3.5	34,562	0.49	86
TRI 49–19 I	95	116	1636	1905	0.2	2382	3757	0.3	2909	1.3	78
NECOCLÍ	232	107	2090	2958	2.2	21,750	3341	1.0	10,031	1.17	81
ZAPSURRO	200	77	2165	2461	2.8	28,350	2321	1.1	10,914	1.64	71
RC13–169	42	67	2020	682	1.9	19,404	1758	3.1	30,954	1.07	82
VM12–110	175	73	2125	2702	8.1	80,850	1820	3.4	33,726	0.19	86
RC09–052	25	57	2075	395	1.2	11,550	1456	2.6	26,334	0.43	95
VM20–012	62	62	2558	795	0.6	6138	1284	0.6	6138	0.35	97
RC11–239	66	50	2635	822	0.7	6534	1006	0.5	4950	0.36	96
PALOMINO4	239	103	2041	4009	11.0	11,0418	2563	4.8	47,586	0.84	75
POPOYA13	102	194	2132	1638	4.7	47,124	4621	9.0	89,628	0.32	98
VM28–07	55	55	4471	404	0.5	5156	604	0.5	5156	0.7	80
RC09–045	31	66	2135	476	1.4	14,322	1638	3.0	30,492	0.49	89
VM24–031	17	58	2232	250	0.2	1683	1377	0.6	5742	0.55	100
VM24–032	63	71	2751	751	0.6	5906	1368	0.7	6656	0.26	93
VM19–017	46	74	2917	517	2.1	21,252	1235	3.4	34,188	0.36	92
POPOYA9	22	70	1255	600	1.0	10,164	2590	3.2	32,340	0.72	91
RINCÓN MAR3	147	54	2550	1529	1.5	14,553	1388	0.5	5346	0.59	91
RC13–148	61	51	3910	512	0.6	5718	691	0.5	4781	0.48	92
C.DIQUE	374	57	3415	3593	3.7	37,026	869	0.6	5643	0.88	56
BERRUGAS16	104	54	2335	1187	1.0	10,296	1509	0.5	5346	1.23	80
EGORO1	393	111	585	22,766	1.4	13,755	2192	0.4	3535	1.46	78
EGORO5	454	80	1268	12,134	1.7	16,684	1942	0.7	7276	1.56	72
EGORO7	297	138	1045	9631	1.1	10,914	1510	0.4	4079	1.5	79
EGORO12	682	54	902	25,623	2.4	23,870	1166	0.3	2800	0.64	95
EGORO15	507	142	2915	5894	1.9	18,632	651	0.5	5071	1.14	79
EGORO14	240	138	1032	7881	0.9	8820	721	0.2	1984	0.94	91
EGORO16	304	210	1126	9149	1.4	14,470	1754	0.7	6759	1.19	77
EGORO17	380	359	1720	7487	1.4	13,965	1007	0.5	5071	1.06	80
EGORO9	450	209	1012	15,069	1.6	15,750	2699	0.7	7350	1.15	72
EGORO20	290	175	902	10,895	1.1	10,657	5162	1.3	13,193	0.88	82
MERA2	534	120	1165	7138	1.1	10,680	5055	0.4	4180	0.75	92
MERA3	420	199	1140	5738	0.9	8820	4235	0.4	3675	0.98	78
MERA5	333	92	1280	8103	0.7	6660	5277	0.2	2400	0.69	78
MERA8	453	132	2960	4767	0.9	9060	3790	0.4	3980	0.51	95
MERA13	279	112	4172	2083	0.6	5580	1231	0.2	1840	1.21	87
VM20–015	87	167	2380	1280	2.3	22,837	2836	3.5	34,650	0.84	89
VM15–011	194	250	2575	2639	0.4	4074	2101	0.2	2352	0.95	84
RC10–253	189	142	2085	3175	0.4	3969	4000	0.4	3507	1.28	69
RC9–065	241	126	2395	3524	0.5	5061	5161	0.5	5250	1.07	82
VM21–216	474	348	3800	4369	1.0	9954	1842	0.3	2982	1	53
KAMA3	191	319	2470	2708	0.4	3820	2592	0.3	2520	1.18	72
KAMA14	292	130	2225	4596	0.6	6132	7987	0.7	7308	1.07	89
KAMA24	228	189	2097	3808	0.5	4560	7740	0.6	6380	1	87
KAMA1	255	254	2329	3835	0.6	6375	2749	0.3	3250	1.14	79
KAMA2	188	224	2180	3020	0.5	4700	4440	0.5	4725	1.33	80
KNR176–2 JPC9	188	146	3802	1732	0.4	3760	3421	0.5	5080	1.05	85
KNR176–2-JPC32	340	130	2612	2280	0.7	6800	2242	0.4	4480	1.15	83
KNR176–2-MC4	412	58	2496	2891	0.8	8240	1452	0.3	2920	0.87	72

and Limoges et al. (2013) (Tables 5 and 6). The heterotrophic/autotrophic (H/A) % was calculated as the number of heterotrophic dinocysts found in the sample divided by the total number of dinocysts in a sample multiplied by 100.

All statistical analyses were performed using the vegan R package (Oksanen et al., 2014; R core Team, 2015).

4. Results and discussion

4.1. Dinocyst, pollen, and spore concentrations and accumulation rates

Dinocyst concentrations in the SC range from 604 to 4621 cysts per gram of dry sediment (mean = 1979 ± 1688), whereas in the ETP, the absolute concentration of cysts per gram of dry sediment ranges from 651 to 7987 (mean = 3105 ± 1956) (Table 5, Figs. 5a, 6). The lower concentration of dinocysts in the SC compared to the ETP can be explained by: 1) the predominance of silt and sand grains in the SC (i.e., coarser grain size) compared to the more clayey substrate of the ETP (Narale et al., 2013); 2) differences in primary productivity, which are considerably higher in the ETP (e.g., Lewis et al., 1990; Dale, 2001; Radi and de Vernal, 2004; Sangiorgi and Donders, 2004; Zonneveld et al., 2010; Hardy et al., 2016; Bringué et al., 2019; de Vernal et al., 2020); and/or 3) differences in the accumulation rate of sediments between the SC and the ETP.

Pollen and spores are very abundant in the studied samples, especially in the ETP samples (Fig. 5b, 6). Pollen and spore concentrations in

Table 6
Dinocyst species recorded in the southern Caribbean (SC) Sea and the eastern tropical Pacific Ocean (ETP), their corresponding plate and map numbers, trophic habit of the corresponding motile stage. A = Autotrophic, H = heterotrophic as determined by Schnepf and Elbrächter (1992) and Limoges et al., (2010), (%): Relative abundance of dinocyst taxa for the fifty-two samples analyzed in this work (Code: Abbreviation name, Fig. 9). Species in bold correspond to the most representative taxa (relative abundance >1%). * = taxon is reported but not mapped.

Cyst name	Plate	Map	Trophism	Motile stage name (Head, 1996)	%	Code
Bitectatodinium spongium	I	Fig. 10	Autotrophic	Unknown	14	BSPO
***Brigantedinium* spp.**	I	Fig. 11	Heterotrophic	*Protoperidinium* sp.	70	BSPP
*Brigantedinium cariacoense**	I	No map	Heterotrophic	*Protoperidinium avellanum*		BCAR
*Brigantedinium simplex**	I	No map	Heterotrophic	*Protoperidinium conicoides*		BSIM
Cyst of *Archaeperidinium bailongense**	I	No map	Heterotrophic	*Archaeperidinium bailongense*	0.3	ABAI
Cyst of *Archaeperidinium constrictum**	I	No map	Heterotrophic	*Archaeperidinium constrictum*	0.2	ACON
Cyst of *Polykrikos schwartzii**	I	No map	Heterotrophic	*Polykrikos kofoidii*	0.7	PSCH
Cyst of *Protoceratium reticulatum*	I	Fig. 12	Autotrophic	*Protoceratium reticulatum*	2	PRET
Echinidinium aculeatum	I	Fig. 13	Heterotrophic	Unknown	5	EACU
*Echinidinium granulatum**	I	No map	Heterotrophic	Unknown	0.9	EGRA
Echinidinium spp.*	I	No map	Heterotrophic	Unknown	0.5	ESPP
*Impagidinium aculeatum**	I	No map	Autotrophic	*Gonyaulax* sp. indet	0.1	IACU
*Lingulodinium machaerophorum**	II	No map	Autotrophic	*Lingulodinium polyedra*	0.2	LMAC
Lejeunecysta sp.*	II	No map	Heterotrophic	Unknown	0.01	LESP
*Nematosphaeropsis lemniscata **	II	No map	Autotrophic	*Gonyaulax spinifera* complex	0.3	NLEM
*Operculodinium israelianum**	II	No map	Autotrophic	*Protoceratium* sp.	0.3	OISR
Selenopemphix nephroides	II	Fig. 14	Heterotrophic	*Protoperidinium subinerme*	4	SNEP
*Selenopemphix quanta**	II	No map	Heterotrophic	*Protoperidinium conicum*	0.5	SQUA
***Spiniferites* spp.**	II	Fig. 15	Autotrophic	*Gonayaulax* spp.	2	SSPP
*Spiniferites bentorii**	II	No map	Autotrophic	*Gonyaulax digitale*		SBEN
*Spiniferites mirabilis**	II	No map	Autotrophic	*Gonyaulax* spinifera complex		SMIR
*Spiniferites pachydermus**	II	No map	Autotrophic	*Gonyaulax* spinifera complex.		SPAC
*Spiniferites ramosus**	II	No map	Autotrophic	*Gonyaulax* spinifera complex.		SRAM
*Stelladinium bifurcatum**	II	No map	Heterotrophic	Unknown	0.06	SBIF
*Tuberculodinium vancampoae**	II	No map	Autotrophic	*Pyrophacus steinii*	0.08	TVAN
*Votadinium spinosum**	II	No map	Heterotrophic	*Protoperidinium claudicans*	0.1	VSPI
Votadinium sp.*	–	No map	Heterotrophic	*Protoperidinium* sp.	0.09	VSPP

the SC range from 250 to 4570 palynomorphs per gram of dry sediment (mean = 1635 ± 5172). In the ETP, pollen and spore concentrations range from 1280 to 25,623 (mean = 6936 ± 5963) (Table 5, Figs. 5b, 6). The higher concentration of terrestrial palynomorphs in the ETP can be explained by: 1) the proximity of many samples to the coast; and 2) the general morphology of the rivers that flow into the ETP that are characterized by their shortness, steepness, and the absence of alluvial floodplains. All together the fluvial morphology of rivers draining the ETP makes it easier for terrestrial palynomorphs to be readily deposited in the basin without being entrapped in proximal areas before reaching the ocean (Restrepo and Kjerfve, 2004).

4.2. Dinocyst assemblages

A total of twenty dinocyst taxa were found in the SC and the ETP (total dinocyst diversity is of 24, but we expose 20 taxa since some groups have been made) (Table 6; Plates I-II). The assemblages consisted of the autotrophic species *Bitectatodinium spongium* and *Spiniferites* spp., and the heterotrophic *Brigantedinium* spp. (the most dominant cyst), and the cysts of *Protoceratium reticulatum*, *Echinidinium aculeatum,* and *Selenopemphix nephroides.* These species represented 94% of the total dinocyst assemblages (Table 6; see Section 5 for a detailed discussion of these most abundant dinocysts and their environmental preferences). The dinocyst species *Archaeperidinium constrictum*, *Echinidinium* spp. (except for *E. aculeatum*), *Stelladinium bifurcatum*, *Votadinium* sp., *Votadinium spinosum*, and *Lejeunecysta* sp. were found in very low numbers or recorded as single occurrences (Fig. 6; Table 4). The relative abundances of these taxa are presented in Figs. 6 and 7, but they will not be further discussed in this paper due to their scarce presence in the assemblages.

4.3. Heterotrophic-autotrophic ratio as an indication of productivity levels

A high heterotrophic/autotrophic (H/A) ratio value has been considered as an indication of high productivity possibly due to high nutrient availability in marine waters (Lewis et al., 1990; Radi and de Vernal, 2004; Sangiorgi and Donders, 2004; Verleye and Louwye, 2010; Zonneveld et al., 2010; Hardy et al., 2016). Based on the modern environmental conditions of the study area, a higher H/A ratio is expected for the ETP (Fig. 6). However, no significant differences in the H/A ratio were observed for the two basins. Conversely and, consistent with the contrasting environmental patterns observed in the ETP and the SC, Huguet et al. (2019) studied the biomarker content of the same surface sediments used in this study and found that the ETP has much higher nutrient levels compared to the more oligotrophic SC. These findings imply that using the H/A ratio in the study area without other proxies can lead to misleading conclusions regarding the nutrient levels. Moreover, if oxygen conditions in bottom water have selectively preserved dinocysts in the samples, the use of the H/A ratio to infer productivity is biased. It is well known that Protoperidiniod cysts (mostly heterotrophic) are more sensitive than G cysts (mostly autotrophic) to oxidation (e.g., Zonneveld et al., 2007, 2010). In locations and/or in down-core records where bottom water oxygen is known to have varied, the use of such a ratio is far from ideal. Such bias can be excluded in our samples (see paragraph 4.4).

4.4. Diversity of dinocyst assemblages

The Shannon-Wiener index (H') was higher in the ETP (mean H' = 1.05 ± 0.24) than in the SC (mean H' = 0.69 ± 0.39) (Fig. 8a; Table 5). Dinocysts, in general, are more abundant and diverse in areas where seasonality and environmental conditions in the water column strongly vary (Dale, 1983). Although distance to the shoreline has an important effect on the dinocyst diversity (Sluijs et al., 2008), the lack of correlation between this parameter and diversity in the study areas is consistent with the higher climatic variability present in the ETP as the main driver of a higher dinocyst diversity compared to the SC.

When samples RC13–100 and VM12–110 from the SC are excluded (*Brigantedinum* spp. concentrations are zero), a significant negative correlation (R^2 = -0.836; $p < 0.001$; Fig. 8b) was found between H' and the relative abundance of *Brigantedinim* spp. A preservation bias can be

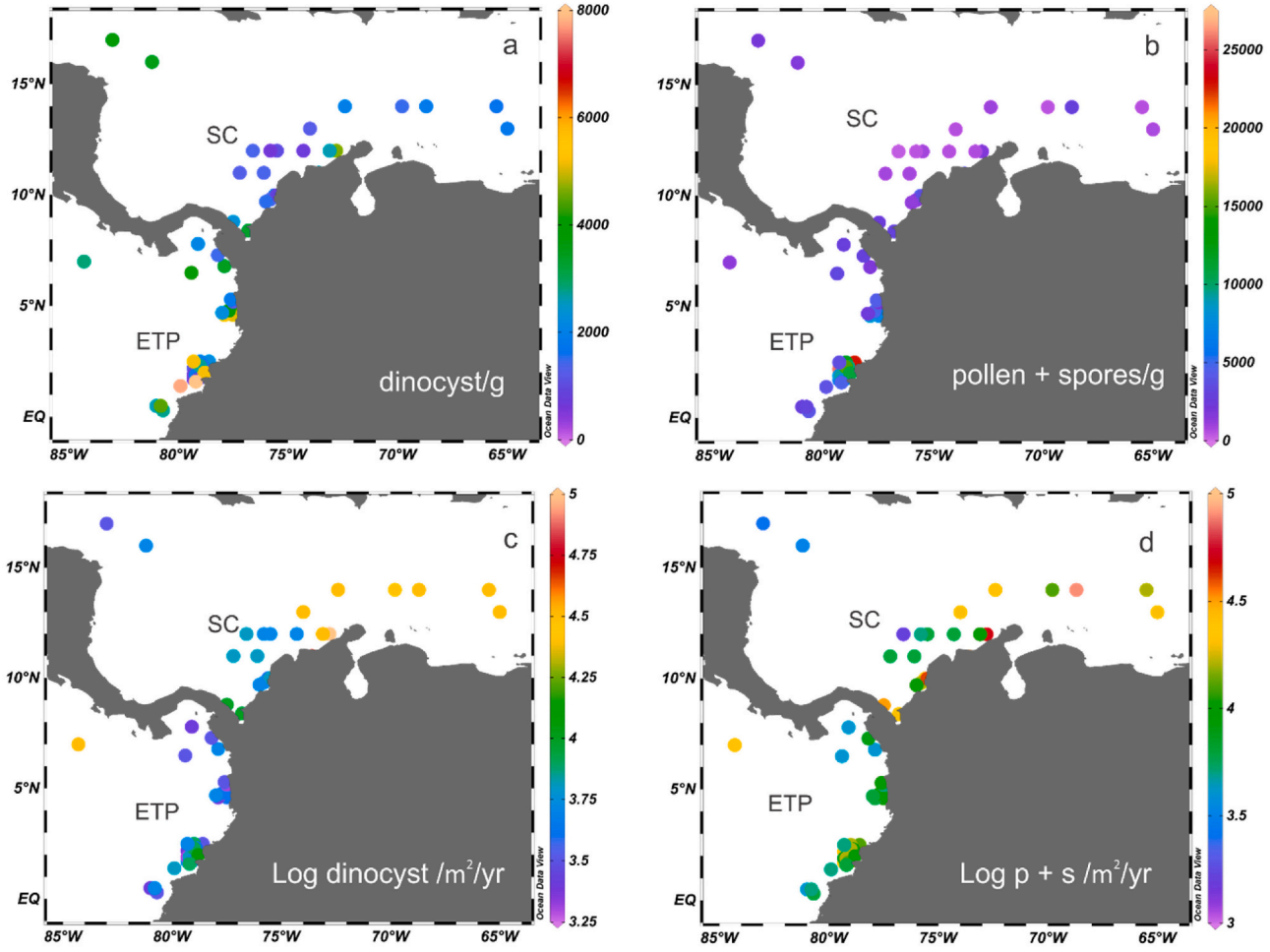

Fig. 5. Geographic distribution of: a- Dinocyst concentration (dinocyst/g), b- concentration of terrestrial palynomorphs (pollen + spores/g), c- flux of dinocysts (Log (dinocyst/m^2/yr.)), d- Log of terrestrial palynomorphs accumulation (Log (pollen + spores/m^2/yr.)) in the southern Caribbean (SC), and eastern tropical Pacific (ETP).

ruled out as *Brigantedinim* spp. is more prone to be oxidized in well-oxygenated environments and therefore be underrepresented in surface sediments when assemblages have been affected by post-depositional processes (Zonneveld et al., 2007). This negative relationship can therefore be explained by the dominance of the *Brigantedinium* group since the *H′* index is sensitive not only to the species richness but also to the evenness of the dinocyst assemblage.

4.5. Environmental parameters related to dinocyst assemblages

Environmental differences between the SC and ETP areas are evident from the different values of the annual mean SST (27.88 °C in the SC and 26.64 °C in the ETP), mean yearly SSS (35.34 psu in the SC and 30.92 psu in the ETP), annual mean [PO_4] (0.035 μmol/L in the SC and. 0.032 μmol/L in the ETP), and seasonal [NO_3]_JFM (0.1 μmol/L in the SC and 1.28 μmol/L in the ETP) (Fig. 3).

The environmental parameters associated with NMDS Axis 1 were [NO_3]_JJA, [NO_3]_JFM, and [PO_4]_JJA. For Axis 2, [NO_3]_JJA and WD drive most of the variation (Table 7). The NMDS plot grouped sample points into two clusters that are clearly related to the geographic location of the samples (Fig. 9a). SC data points are plotted on the left-hand side of the first NMDS axis, whereas all the ETP sediment samples are plotted on the right-hand side of the first axis (Fig. 9a, Table 7).

The SC samples are scattered along axis 2 and can be further subdivided into two subgroups (SC-1 and SC-2) in the NMDS plot (Fig. 9a). The first subgroup (SC-1) is represented by seventeen data points containing the samples collected from the deepest parts of the SC region and therefore these samples have very limited riverine influence. The SC-2 subgroup, on the other hand, included seven samples collected in areas under the influence of the Atrato and Magdalena Rivers or in their embayments (i.e. Berrugas 16, Rincon del Mar, Necocli, and Zapsurro).

4.6. Environmental data as drivers of the most common species

Seventy-seven per cent of the total variance in the data is explained by the environmental data and the relative abundance of dinocysts (Fig. 9; Axis 1 = 57% and Axis 2 = 20%). Based on the RDA, seasonal and annual SSS [PO_4], and [NO_3] are the most important variables controlling the differences in the dinocyst abundances in the SC and the ETP (Fig. 9b, Table 8). SSS Annual and in JJA were negatively related to RDA axis 1. *Brigantedinium* spp., the cysts of *P. reticulatum*, *S. nephroides,* and *Spiniferites* spp. plot towards the center of the first axis, while *B. spongium* and *E. aculeatum* plotted on the right-hand side of the RDA reflecting a first order control of the SSS values on the abundance of these species (Fig. 9b). SSS Annual and in JJA are negatively related to RDA Axis 1. Axis 1 is defined by negative RDA scores for *Brigantedinium* spp., the cysts of *P. reticulatum*, *S. nephroides,* and *Spiniferites* spp., and by positive scores for *B. spongium* and *E. aculeatum* (Fig. 9b, Table 8). In contrast, *Brigantedinium* spp. is positively related to RDA Axis 2, plotted in a more negative position compared to the other species that dominate the assemblages (Fig. 9b, Table 8).

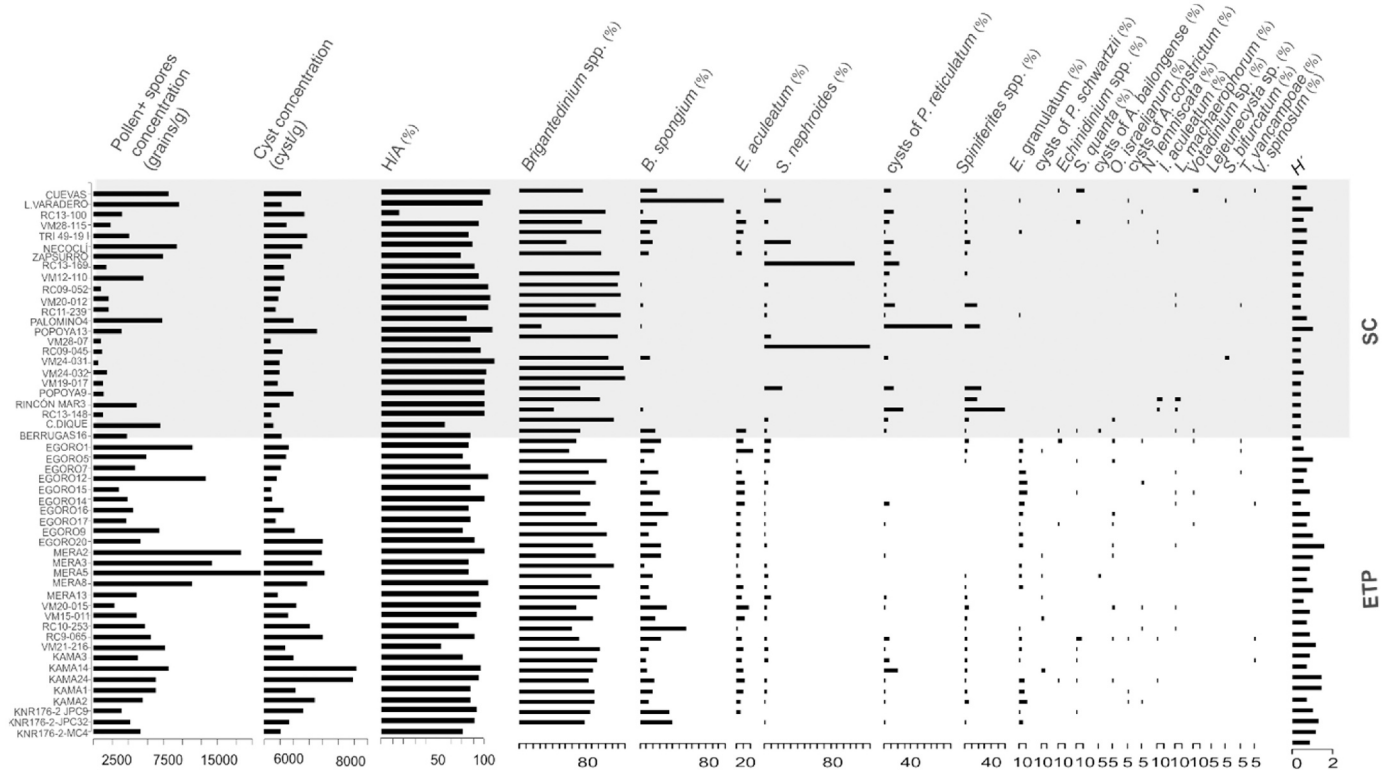

Fig. 6. From left to right: Pollen grains and spore concentrations per gram of dry sediment (pollen +spores/g). Dinocyst concentration per gram dry sediment (cyst/g). Heterotrophic/Autotrophic ratio (H/A). Relative abundances of dominant and rare dinocyst taxa and Shannon–Wiener index (*H'*). The grey rectangle highlights the southern Caribbean; the white background represents the eastern tropical Pacific.

5. Occurrences and environmental requirements of the most abundant dinocyst taxa

The following section presents a discussion of the distribution and abundance patterns of the dominant taxa in the dinocyst assemblages and their preferred environmental conditions in the SC and ETP zones.

5.1. *Bitectatodinium spongium Zonneveld, KAF and Jurkschat et al., (1999), Figs. 10, 16a, Plate I, 1–2*

Distribution: *Bitectatodiniumspongium* was found to be a common cyst in the ETP and a minor component of the dinocyst assemblages in the SC. This species was the second most abundant taxon in the studied samples representing 14% of the SC and ETP cyst assemblage. The highest abundances of the cyst were found in the ETP associated with upwelling zones (Figs. 10a). The low abundance of cysts found in modern sediments of the SC zone are at odds with high-production rates of the cyst that have been reported from sediment traps in the Cariaco Basin (Bringué et al., 2019). The highest abundances of *B. spongium* in the study area were observed at annual temperatures above 27 °C and salinity of 28 psu and 36 psu. The highest values of the cyst in the study area are positively correlated with [PO_4] and [NO_3]. The preferred SST, SSS, [PO_4], and [NO_3] values reported here for *B. spongium* are in good agreement with previous environmental ranges reported for the species (Zonneveld et al., 2013).

On a global scale, the highest abundances of *B. spongium* have been found in nutrient-rich waters and upwelling zones (Zonneveld and Jurkschat, 1999; Zonneveld and Pospelova, 2015). For the tropics, Bringué et al. (2019) found the highest abundances of *B. spongium* following seasonal episodes of intense upwelling in the Cariaco Basin. Also, Limoges et al. (2010) and Vásquez-Bedoya et al. (2008) found *B. spongium* along the southwestern coast of Mexico and in the Gulf of Tehuantepec areas with seasonal upwelling. In the SC and the ETP, areas dominated by *B. spongium* were similarly associated with upwelling zones.

5.2. *Brigantedinium spp. Figs. 11, 16b; Plate I, 3–4*

Morphological remark: *Brigantedinium simplex*, *Brigantedinium cariacoense*, and other undetermined species of the genus *Brigantedinium* were grouped as *Brigantedinium* spp.

Distribution: *Brigantedinium* spp. were the most abundant species of cysts in both the ETP and the SC. The abundances of *Brigantedinium* spp. increased when [NO_3] were at the lowest annual average (0.1 μmol/L). This group of species represents 70% of the total number of cysts found in the ETP and the SC. *Brigantedinium* spp. were found through a wide range of water depths (mean = 1326 m, sd = 1319, min = 1 m, max = 4649 m). The highest quantities of *Brigantedinium* spp. were found when annual SST > 26 °C. In sediment traps of the Cariaco Basin, *Brigantedinium* spp. is very abundant (ca. 59%) in modern assemblages with a maximal annual cyst production from December to May coinciding with active upwelling (Bringué et al., 2019).

On a global scale, the highest abundances of *Brigantedinium* spp. have been found in upwelling zones, with increasing abundance when upwelling is active and decreasing abundance during upwelling relaxation (de Vernal et al., 2020). Limoges et al. (2010) and Vásquez-Bedoya et al. (2008) recorded a widespread distribution of *Brigantedinium* spp. along the Mexican coast and the lowest abundances in nearshore environments. Based on the global distribution of this taxon, *Brigantedinium* spp. can be considered cosmopolitan. Its presence has been reported from the tropics to regions permanently covered by sea ice and in water depths that range from coastal areas to the deep ocean (de Vernal et al., 1997; Marret and Zonneveld, 2003; Pospelova et al., 2008, 2010; Zonneveld et al., 2013).

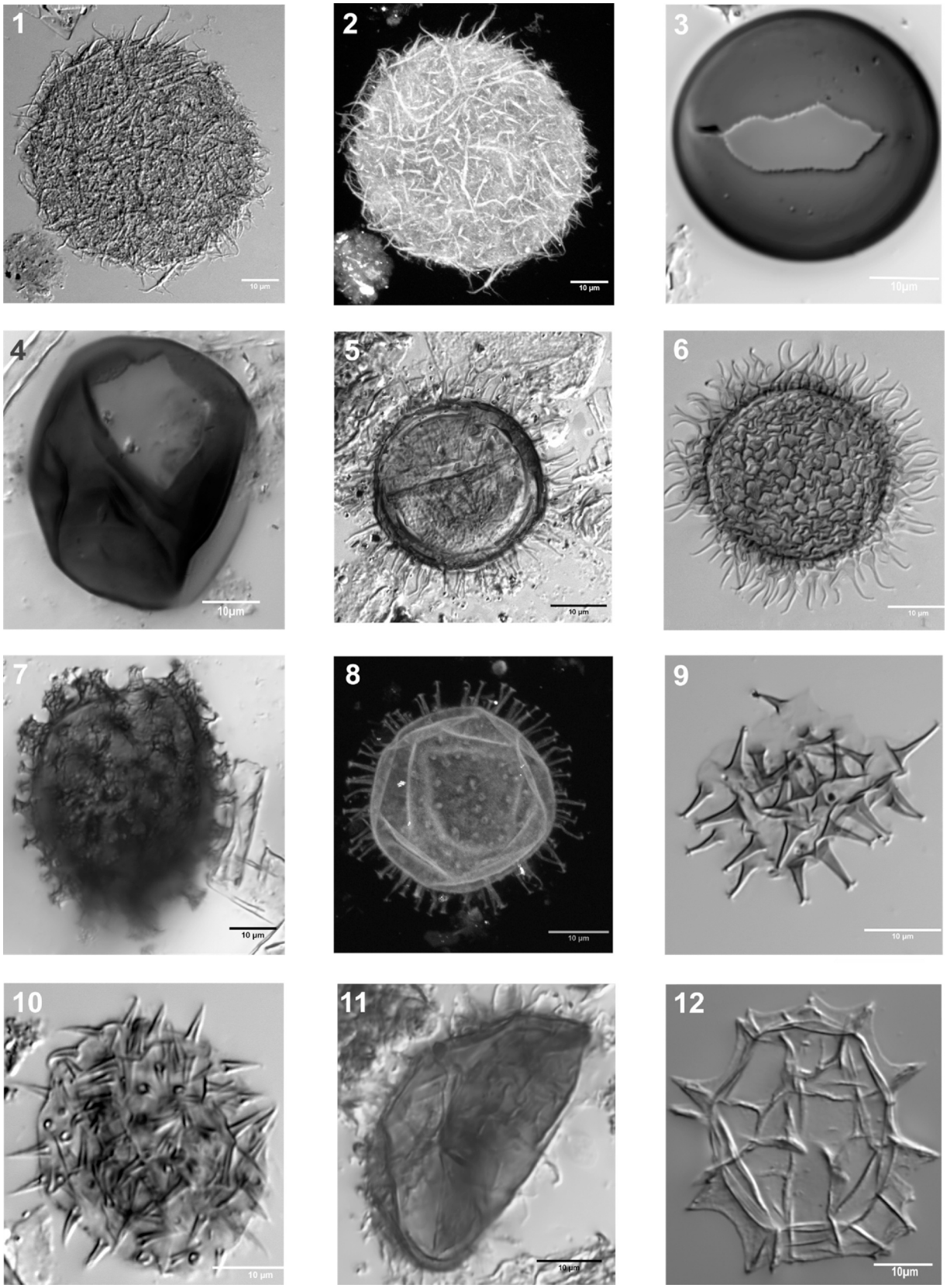

Plate I. 1–2: *Bitectatodinium spongium*; 3–4: *Brigantedinium* spp.; 5: *Archaeperidinium bailongense*; 6: cysts of *Archaeperidinium constrictum*; 7: cysts of *Polykrikos schwartzii*; 8: cysts of *Protoceratium reticulatum*; 9: *Echinidinium aculeatum*; 10: *Echinidinium granulatum*. 11: *Echinidinium* spp.; 12: *Impagidinium aculeatum*. Scale bar = 10 μm.

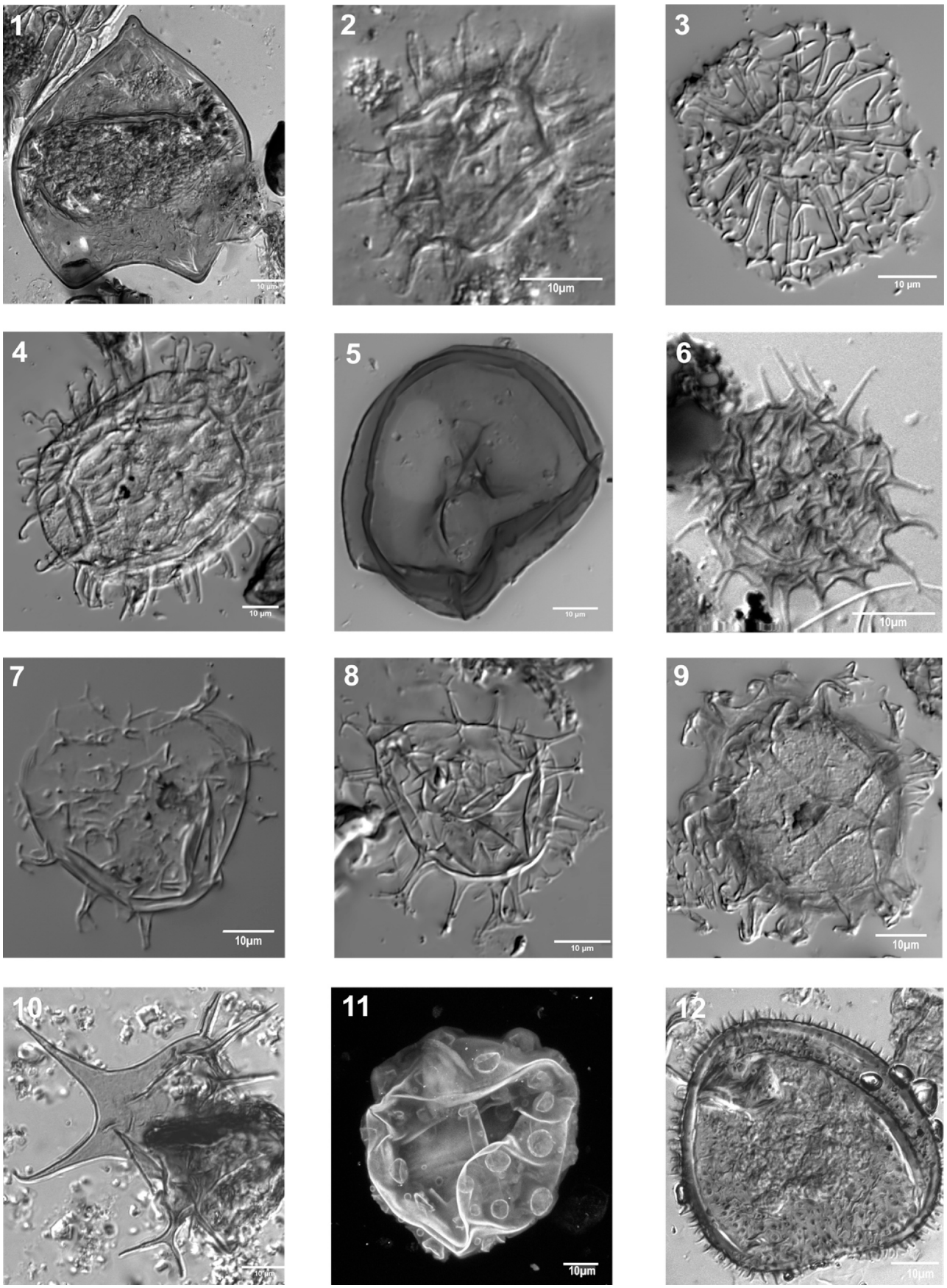

Plate II. 1: *Lejeunecysta* sp.; 2: *Lingulodinium machaerophorum*; 3: *Nematosphaeropsis lemniscata*; 4: *Operculodinium israelianum*; 5: *Selenopemphix nephroides*; 6: *Selenopemphix quanta*; 7–8: *Spiniferites* spp.; 9: *Spiniferites* spp.; 10: *Stelladinium bifurcatum*, 11: *Tuberculodinium vancampoae*; 12: *Votadinium spinosum*. Scale bar = 10 µm.

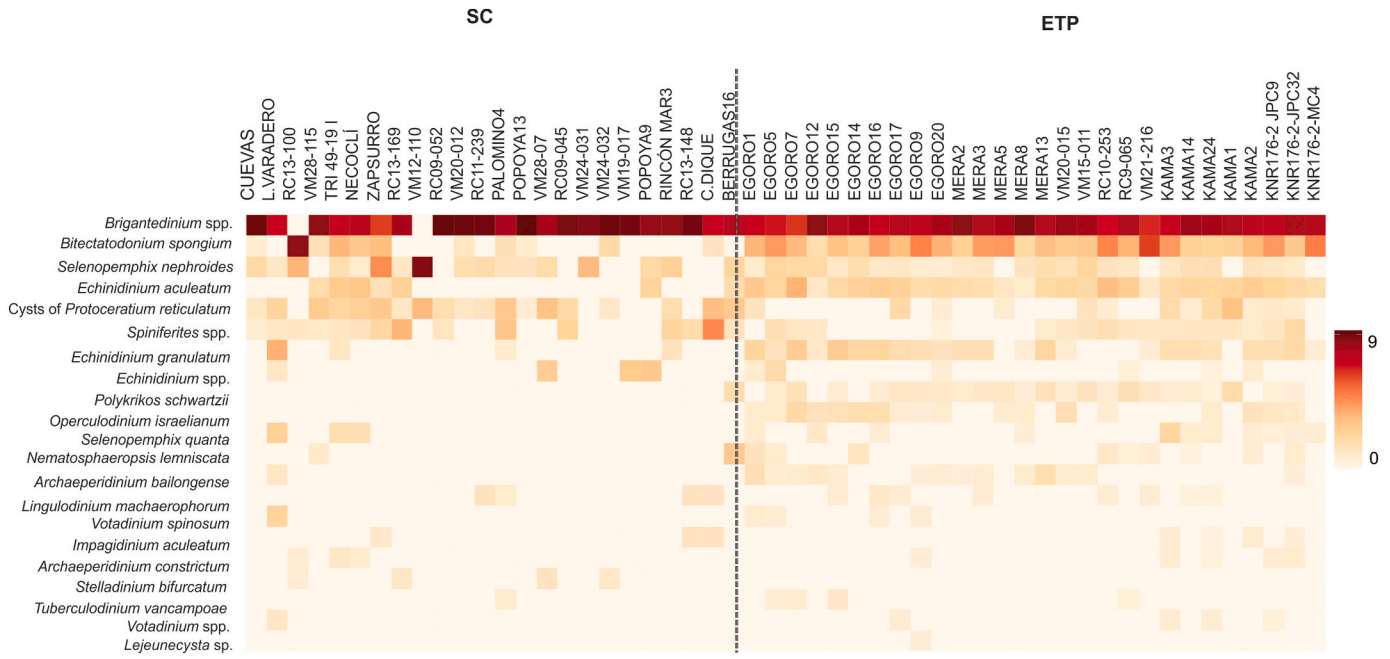

Fig. 7. Shade plot of square root transformed dinocyst relative abundances for the southern Caribbean (SC) and eastern tropical Pacific (ETP). Highest abundances are shown in dark orange and lowest transformed relative abundances are shown in light orange.

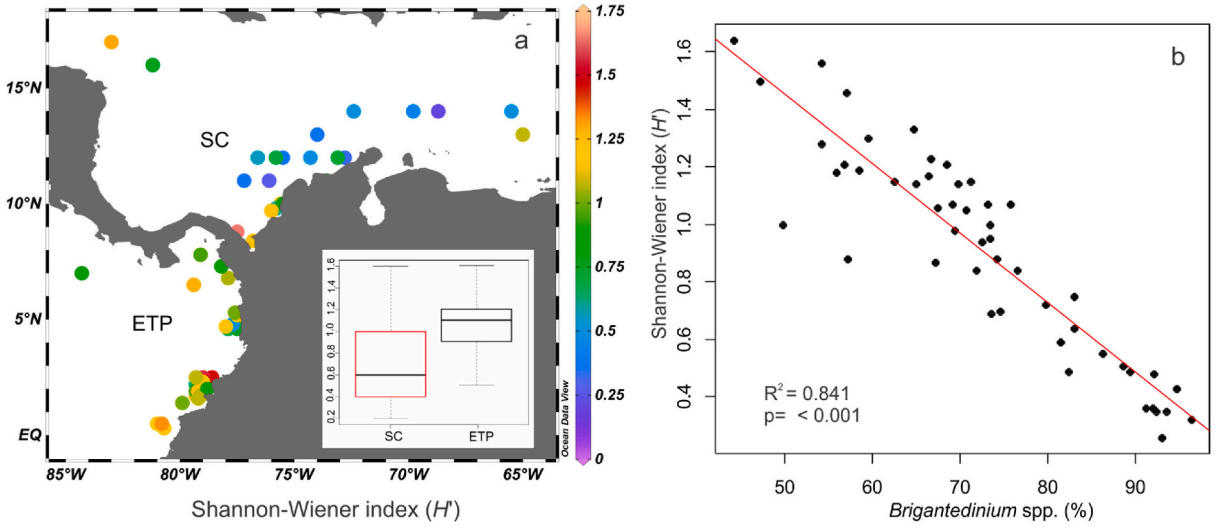

Fig. 8. a- The Shannon-Wiener diversity index (*H'*) of dinocysts. The insert figure shows box plots for the southern Caribbean (red box) and the ETP (black box). b- Biplot of the Shannon-Wiener index (*H'*) and *Brigantedinium* spp. relative abundances.

5.3. Cysts of Protoceratium reticulatum (Claparède and Lachmann, 1859) Bűttschli, 1885, Figs.12, 16c; Plate I, 8. Morphological remark: Following Paez-Reyes and Head (2013), cysts with similar morphology to Operculodinium centrocarpum sensu Wall and Dale, 1966 are referred to in this paper as cysts of Protoceratium reticulatum

Distribution: Cysts of *Protoceratium reticulatum* were more abundant in the SC than in the ETP, with the highest abundances in the SC being related to areas with high SSS values. This species represented 2% of the entire cyst assemblages of the SC and the ETP and the cysts of *Protoceratium reticulatum* were observed in sediments deposited over a wide range of water depths (mean of =1708 m, sd = 1698, min = 1 m max = 5040 m).

The highest abundances of cysts of *Protoceratium reticulatum* were found where annual temperatures range from 27 °C to 29 °C and with SSS at 35 psu and above 36.8 psu.

The cysts of *Protoceratium reticulatum* recorded in the SC and the ETP show a morphological variation expressed as changes in the length of the processes, which ranged from 2.7 μm to 9.4 μm with an average length of 5.53 μm and a standard deviation of 1.56 μm for twenty-one specimens. Mertens et al. (2011) and Verleye et al. (2012) demonstrated that the length of the processes in this species is controlled mainly by salinity and temperature. However, its genetic variation and the presence of pseudo-cryptic species, means that its use as an environmental tracer is not straightforward (Mertens et al., 2011).

Table 7
Scores for axes 1 and 2, according to the non-metric multidimensional scaling (NMDS) of environmental parameters for the southern Caribbean (SC) and eastern tropical Pacific (ETP). Bold numbers correspond to NMDS-scores of most explanatory environmental variables.

Environmental parameter	NMDS1	NMDS2
SST_A	−0.06089072	−0.03252157
SST_JJA	−0.05773889	−0.03205266
SST-JFM	−0.05242172	−0.03229783
SSS_A	−0.07261274	−0.02336757
SSS_JJA	−0.06867755	−0.02783331
SSS_JFM	−0.07378798	−0.02929745
PO4_A	**0.28471409**	−0.02362933
PO4_JJA	**0.37472981**	−0.03265386
PO4_JFM	0.04031442	−0.18018941
NO3_A	**0.26765733**	−0.11289742
NO3_JJA	**−0.67271222**	**0.52257962**
NO3_JFM	**0.53042314**	−0.14296472
WD	−0.00488358	**0.32575543**
DC	−0.05720408	0.29670788

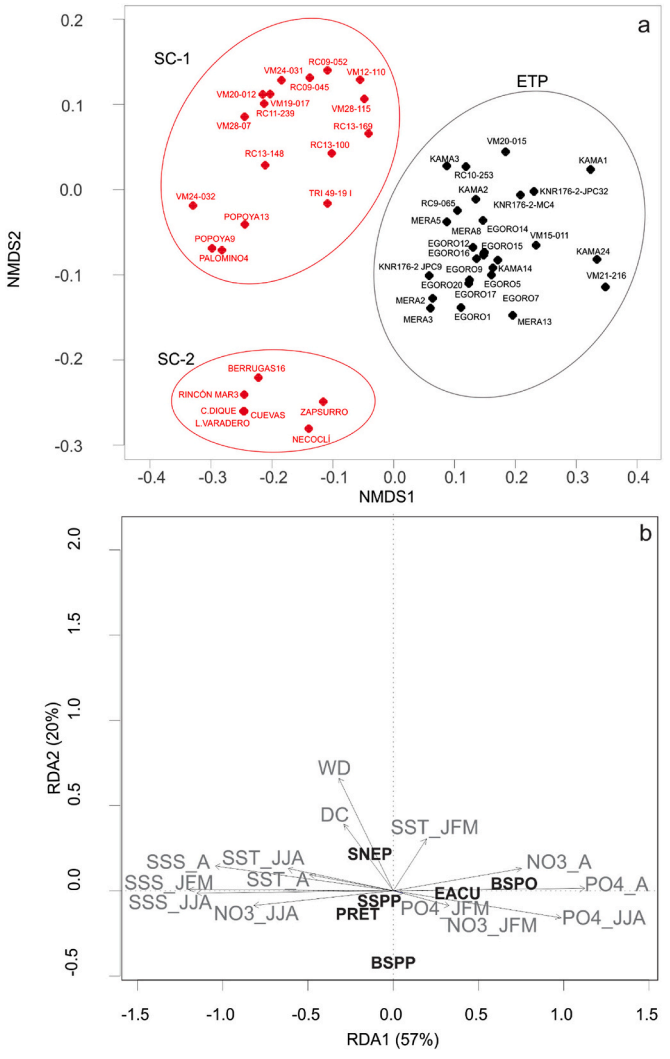

Fig. 9. a- Non-metric multidimensional scaling (NMDS) for environmental parameters based on Bray-Curtis similarities for the southern Caribbean (SC) (red dots) and eastern tropical Pacific (ETP) (black dots); b- Redundancy analysis (RDA) for more abundant species and environmental parameters according to axes 1 and 2 of the variance. Species abbreviations: *Bitectatodinium spongium* (BSPO), *Brigantedinium* spp. (BSPP), cysts of *Protoceratium reticulatum* (PRET), *Echinidinium aculeatum* (EACU), *Selenopemphix nephroides* (SNEP), *Spiniferites* spp. (SSPP).

Table 8
Scores for axes 1 and 2, according to the redundancy analysis (RDA) of the correlation coefficient between the environmental parameters and the scores for the more representative dinocysts. Parameter abbreviations are: sea surface temperature (SST), sea surface salinity (SSS), phosphates concentration ([PO_4]), nitrates concentration ([NO_3]), annual (A), June–July–August (JJA), January–February–, March (JFM). Water depth (WD) and distance to the coast (DC) for the southern Caribbean (SC) and eastern tropical Pacific (ETP). Bold numbers correspond to RDA-scores of most explanatory variables and species.

Environmental parameter	RDA1	RDA2
SST_A	−0.36404	0.070137
SST_JJA	−0.45797	0.095381
SST_JFM	0.14178	0.225984
SSS_A	**−0.77344**	0.107213
SSS_JJA	**−0.85130**	−0.007678
SSS_JFM	**−0.88660**	0.007302
PO4_A	**0.82990**	0.010562
PO4_JJA	**0.72494**	−0.113969
PO4_JFM	0.04251	−0.009680
NO3_A	0.55406	0.096139
NO3_JJA	**−0.60477**	−0.061774
NO3_JFM	0.24242	−0.064725
WD	−0.23448	**0.490224**
DC	−0.21446	**0.291055**
Dinocyst taxa		
Brigantedinium spp.	−0.03801832	**−0.41565202**
Bitectatodinium spongium	**0.67531513**	0.04883838
Echinidinium aculeatum	**0.32477966**	−0.09893145
Cysts of *Protoceratium reticulatum*	−0.24688309	−0.06643120
Selenopemphix nephroides	−0.17706919	**0.22263322**
Spiniferites spp.	−0.11956780	−0.05325828

5.4. *Echinidinium aculeatum* Zonneveld, 1997* Figs. 13, 16d; Plate I, 9.

*Morphological remark: * the name was not validly published in Zonneveld (1997) because the original description of the species based on a modern cyst did not include a latin diagnosis (see discussion in Head, 2002)*

Distribution: *E. aculeatum* was a minor component of the assemblages from the SC but present in almost every sample from the ETP (Fig. 10a). *E. aculeatum* represented 4% of the entire cyst assemblages and was observed in sediments deposited over a wide range of water depths (mean of =1171 ± 1168 m, min = 1 m, max = 4649 m). Although this taxon is only found in low-relative abundances in sediments from the SC compared to the ETP, the cyst has often been reported to be found in sediment traps and sediment cores from the Cariaco Basin with a strong association to upwelling (González et al., 2008; Bringué et al., 2019). Consistent with these observations, the highest abundances of *E. aculeatum* in the study area occurred in close proximity to upwelling zones (Fig. 13a). The peak cyst abundance of *E. aculeatum* was found in the ETP at 32 psu.

On a global scale, the highest abundances of *E. aculeatum* have been found in coastal regions of active upwelling and zones with increased nutrient availability and low-salinity variations (Zonneveld, 1997; Ribeiro and Amorim, 2008; Limoges et al., 2010; Pospelova and Kim, 2010; Zonneveld et al., 2013). Bringué et al. (2019) found that the highest production of *E. aculeatum* in the SC was associated with active but seasonal upwelling in the Cariaco Basin. In the southeast Pacific, *E. aculeatum* appeared to be the best indicator for the presence of year-round active upwelling zones (Verleye and Louwye, 2010). In the Gulf of Mexico, this taxon was observed in nutrient-rich areas and nearby urban centers with extensive industrial activity (Vásquez-Bedoya et al., 2008; Limoges et al., 2010, 2013).

5.5. *Selenopemphix nephroides* (Benedek 1972) Benedek et Sarjeant, 1981, Figs. 14, 16e; Plate II, 5

Distribution: *S. nephroides* was observed in almost all localities analyzed in the SC and the ETP but was generally found in low relative

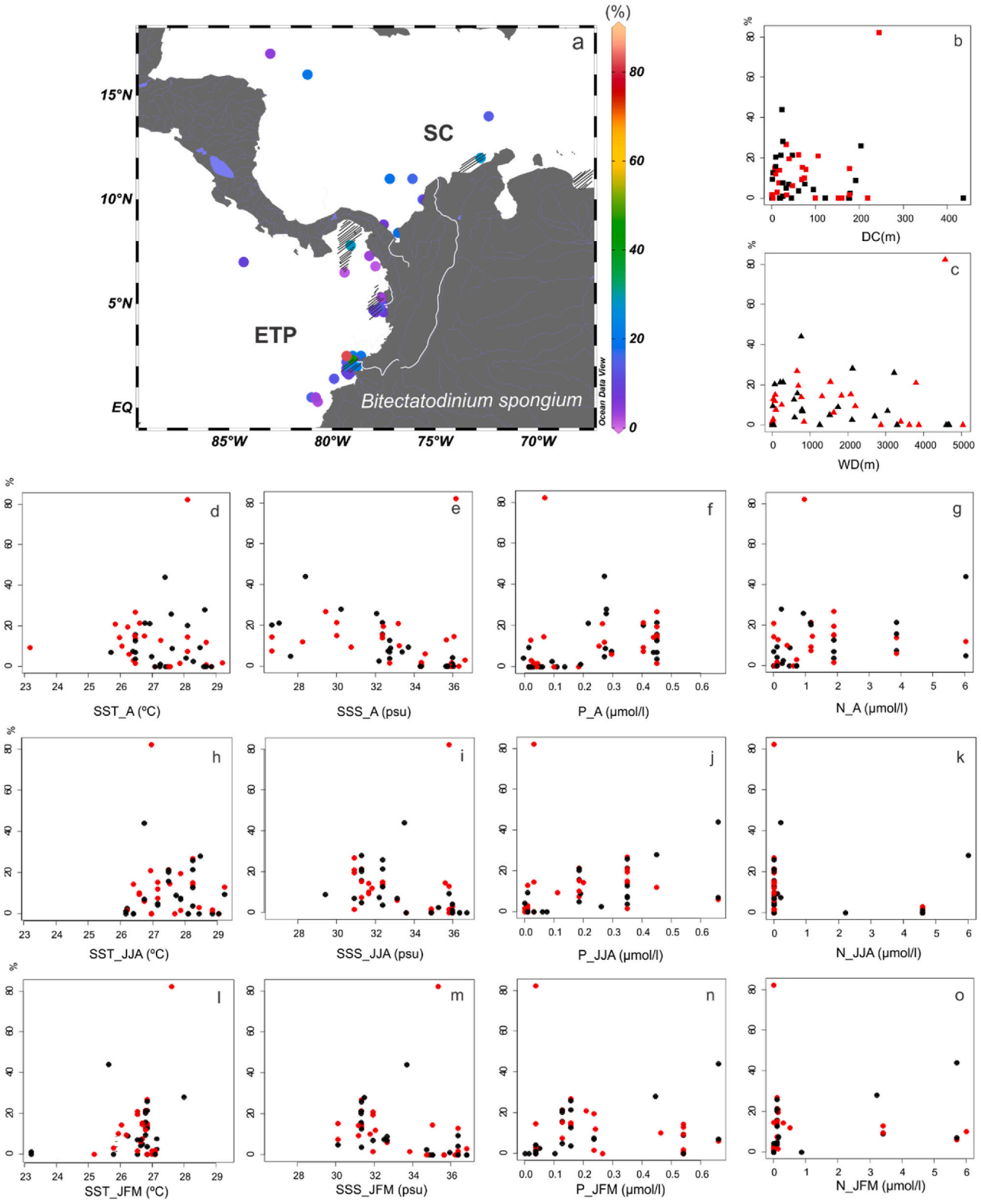

Fig. 10. a- Geographic distribution of *Bitectatodinium spongium,* b- Distance to the coast, c- Water depth, surface-water conditions in the southern Caribbean (SC) and the eastern tropical Pacific (ETP). Sea-surface temperature (SST) in °C: a- Annual (SST_A), h- June–July–August (SST_JJA), l- January–February–March (SST_JFM). Sea-surface salinity (SSS) in psu: e- Annual (SSS_A), i- June–July–August (SSS_JJA), m- January–February–March (SSS_JFM). The sea-surface concentration of phosphates ([PO4]) in µmol/L: f- Annual ([PO4]_A), j- June–July–August ([PO4]_JJA), n- January–February–March ([PO4]_JFM). The sea-surface concentration of nitrates ([NO3]) in µmol/L: g- Annual ([NO3]_A), k- June–July–August ([NO3]_JJA), o- January–February –March ([NO3]_JFM). Values were downloaded from the World Ocean Atlas 2013 (Boyer et al., 2013).

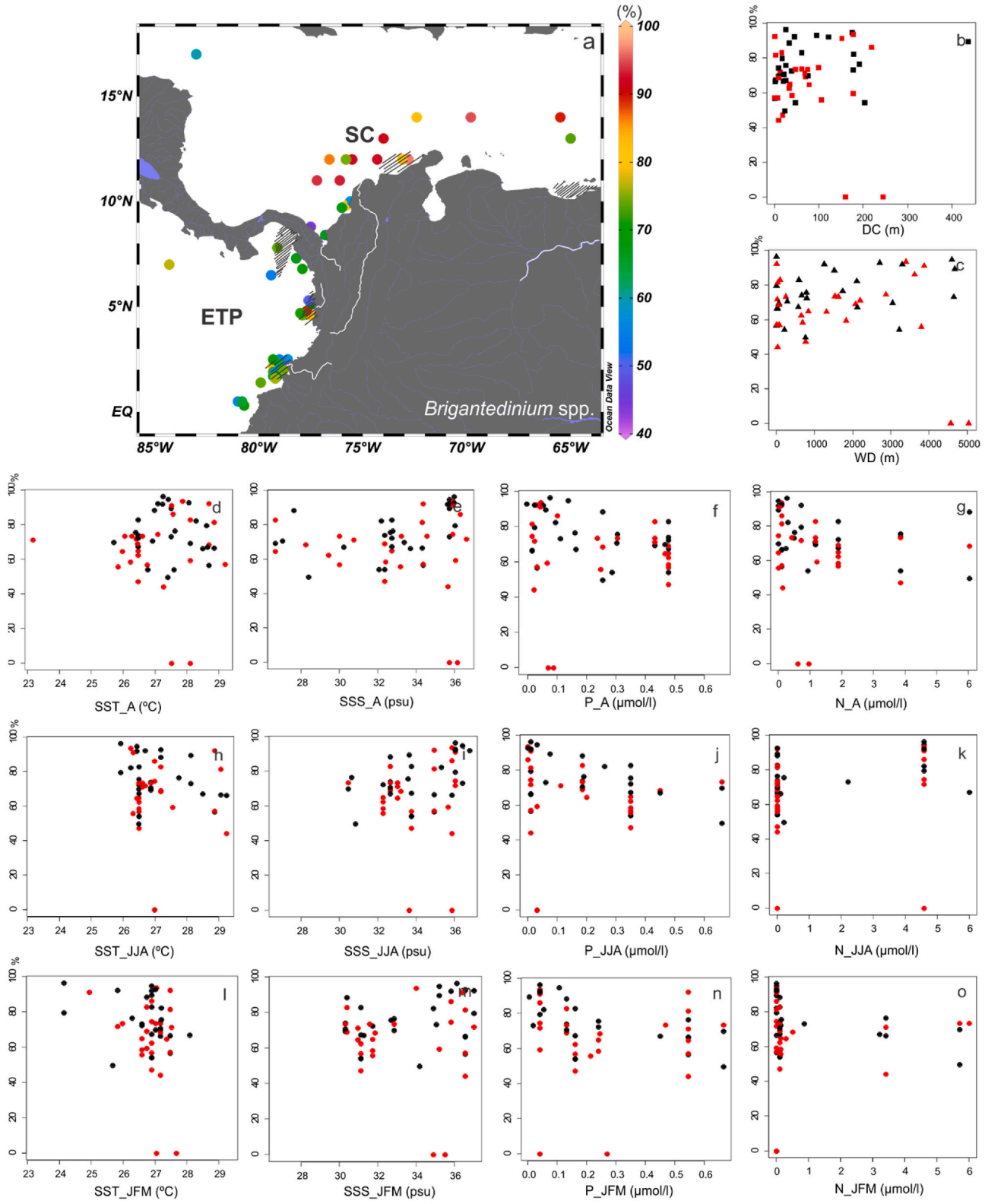

Fig. 11. a- Geographic distribution of *Brigantedinium* spp., b- Distance to the coast, c- Water depth, surface-water conditions in the southern Caribbean (SC) and the eastern tropical Pacific (ETP). Sea-surface temperature (SST) in °C: a- Annual (SST_A), h- June–July –August (SST_JJA), l- January–February –March (SST_JFM). Sea-surface salinity (SSS) in psu: e- Annual (SSS_A), i- June–July–August (SSS_JJA), m- January–February–March (SSS_JFM). The sea-surface concentration of phosphates ([PO4]) in µmol/L: f- Annual ([PO4]_A), j- June–July–August ([PO4]_JJA), n- January–February–March ([PO4]_JFM). The sea-surface concentration of nitrates ([NO3]) in µmol/L: g- Annual ([NO3]_A), k- June–July –August ([NO3]_JJA), o- January–February –March ([NO3]_JFM). Values were downloaded from the World Ocean Atlas 2013 (Boyer et al., 2013).

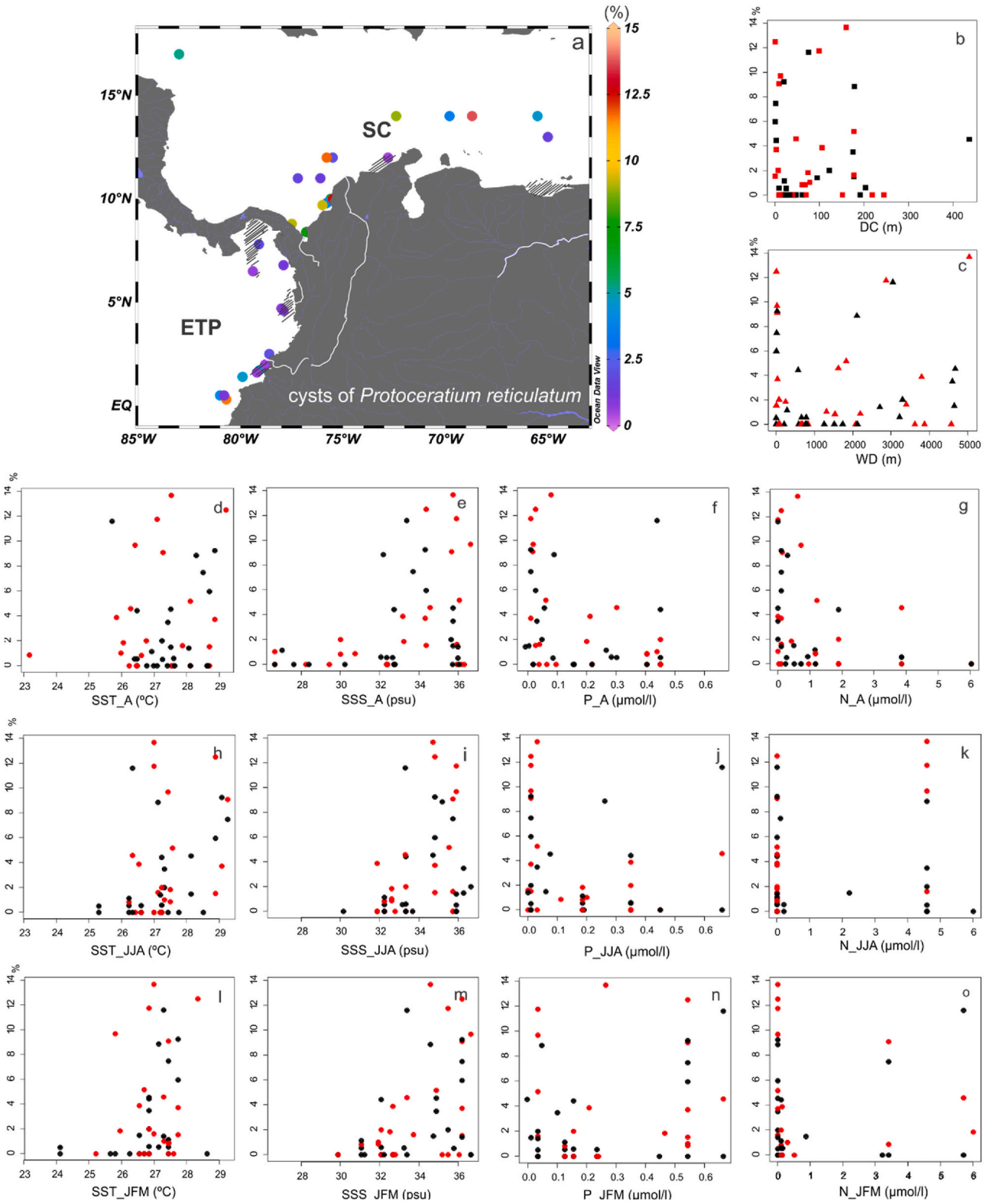

Fig. 12. a- Geographic distribution of cysts of *Protoceratium reticulatum*, b- Distance to the coast, c- Water depth, surface-water conditions in the southern Caribbean (SC) and the eastern tropical Pacific (ETP). Sea-surface temperature (SST) in °C: a- Annual (SST_A), h- June–July–August (SST_JJA), l- January–February–March (SST_JFM). Sea-surface salinity (SSS) in psu: e- Annual (SSS_A), i- June–July–August (SSS_JJA), m- January–February–March (SSS_JFM). The sea-surface concentration of phosphates ([PO4]) in µmol/L: f- Annual ([PO4]_A), j- June–July– August ([PO4]_JJA), n- January–February–March ([PO4]_JFM). The sea-surface concentration of nitrates ([NO3]) in µmol/L: g- Annual ([NO3]_A), k- June–July –August ([NO3]_JJA), o- January–February–March ([NO3]_JFM). Values were downloaded from the World Ocean Atlas 2013 (Boyer et al., 2013).

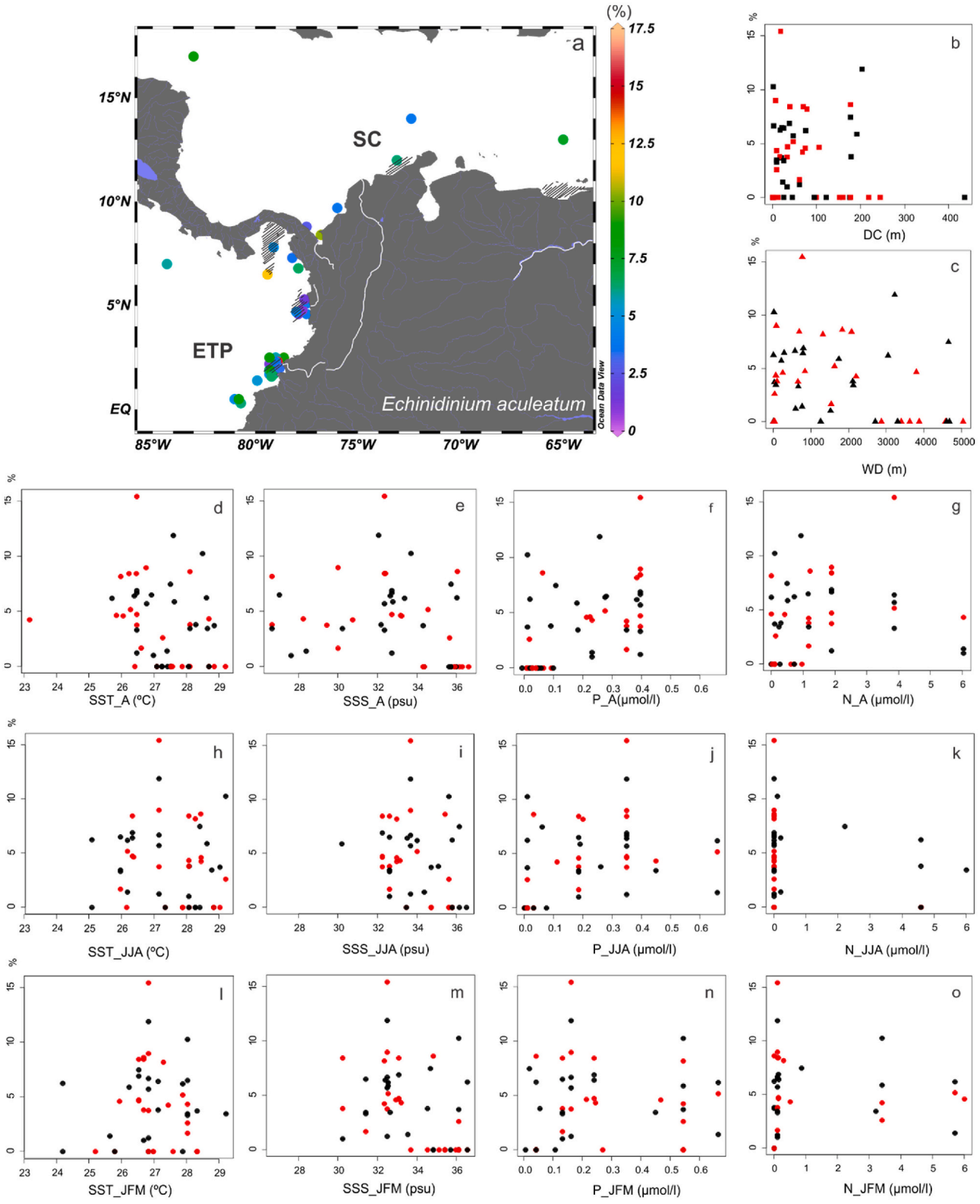

Fig. 13. a- Geographic distribution of *Echinidinium aculeatum*, b- Distance to the coast, c- Water depth, surface-water conditions in the southern Caribbean (SC) and the eastern tropical Pacific (ETP). Sea-surface temperature (SST) in °C: a- Annual (SST_A), h- June–July–August (SST_JJA), l- January–February–March (SST_JFM). Sea-surface salinity (SSS) in psu: e- Annual (SSS_A), i- June–July–August (SSS_JJA), m- January–February–March (SSS_JFM). The sea-surface concentration of phosphates ([PO4]) in µmol/L: f- Annual ([PO4]_A), j- June–July–August ([PO4]_JJA), n- January–February–March ([PO4]_JFM). The sea-surface concentration of nitrates ([NO3]) in µmol/L: g- Annual ([NO3]_A), k- June–July –August ([NO3]_JJA), o- January–February –March ([NO3]_JFM). Values were downloaded from the World Ocean Atlas 2013 (Boyer et al., 2013).

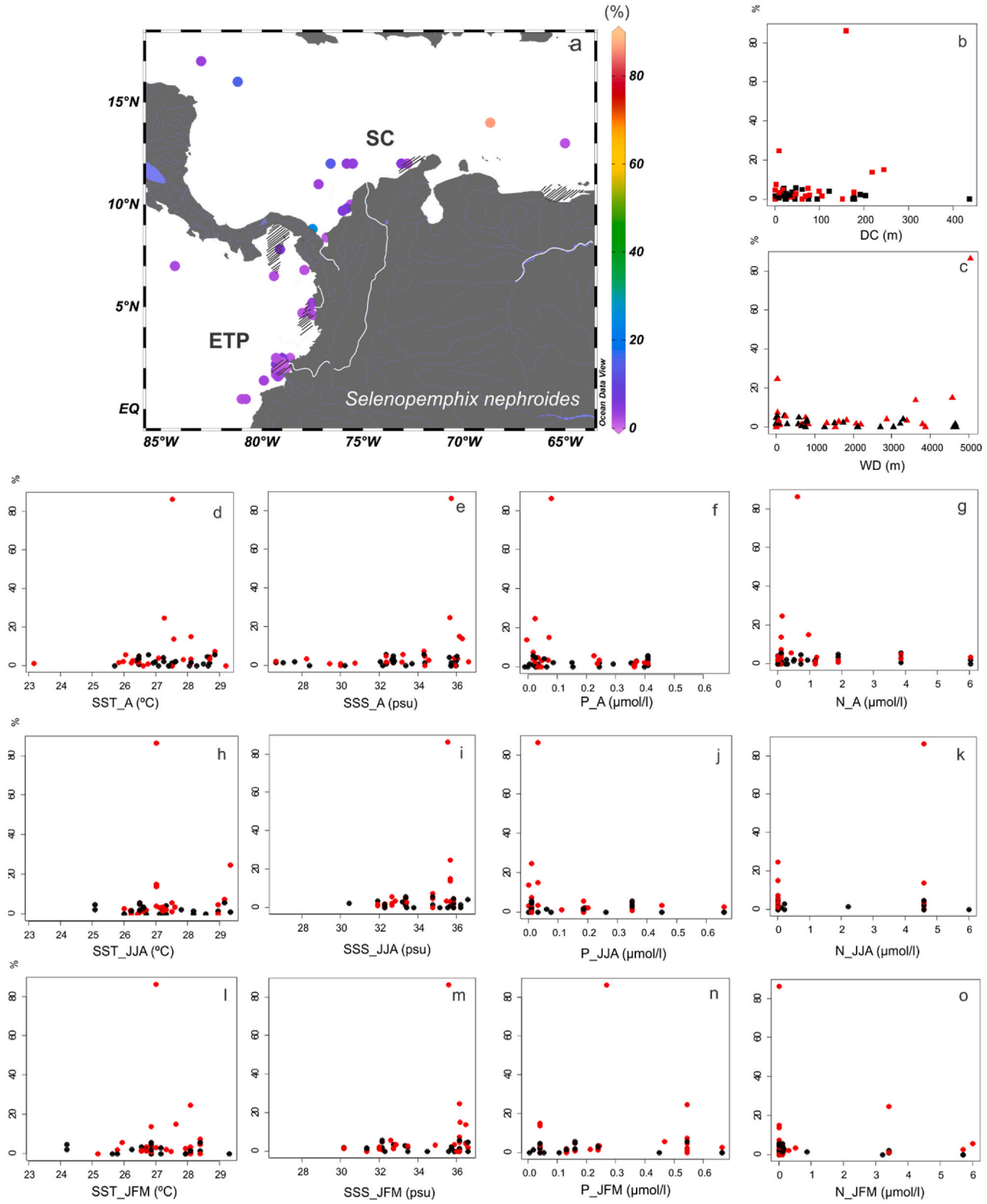

Fig. 14. a- Geographic distribution of *Selenopemphix nephroides*, b- Distance to the coast, c- Water depth, surface-water conditions in the southern Caribbean (SC) and the eastern tropical Pacific (ETP). Sea-surface temperature (SST) in °C: a- Annual (SST_A), h- June–July–August (SST_JJA), l- January–February –March (SST_JFM). Sea-surface salinity (SSS) in psu: e- Annual (SSS_A), i- June–July–August (SSS_JJA), m- January–February–March (SSS_JFM). The sea-surface concentration of phosphates ([PO4]) in µmol/L: f- Annual ([PO4]_A), j- June–July–August ([PO4]_JJA), n- January–February–March ([PO4]_JFM). The sea-surface concentration of nitrates ([NO3]) in µmol/L: g- Annual ([NO3]_A), k- June–July–August ([NO3]_JJA), o- January–February –March ([NO3]_JFM). Values were downloaded from the World Ocean Atlas 2013 (Boyer et al., 2013).

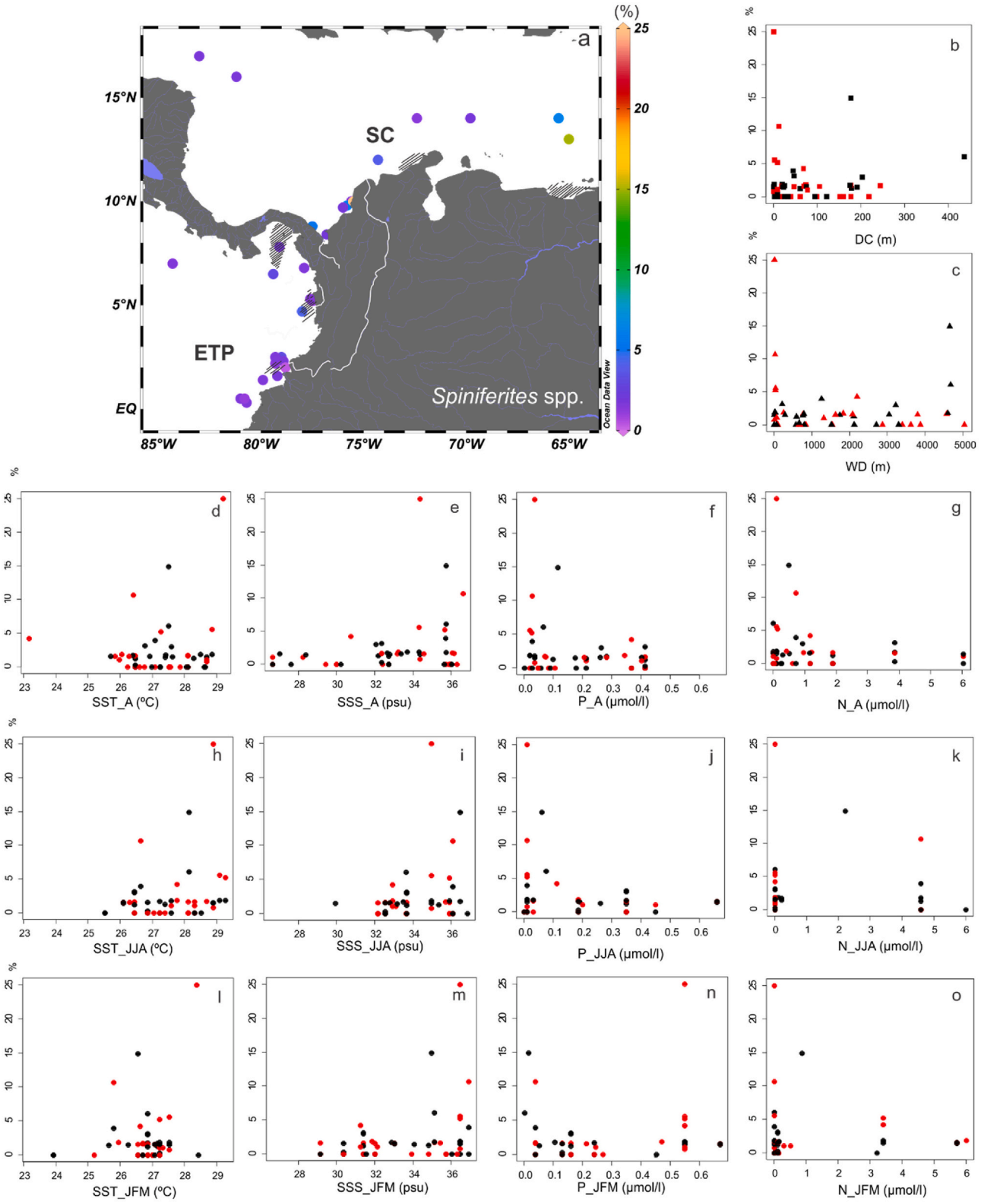

Fig. 15. a- Geographic distribution of *Spiniferites* spp., b- Distance to the coast, c- Water depth, surface-water conditions in the southern Caribbean (SC) and the eastern tropical Pacific (ETP). Sea-surface temperature (SST) in °C: a- Annual (SST_A), h- June–July–August (SST_JJA), l- January–February–March (SST_JFM). Sea-surface salinity (SSS) in psu: e- Annual (SSS_A), i- June–July–August (SSS_JJA), m- January–February–March (SSS_JFM). The sea-surface concentration of phosphates ([PO4]) in µmol/L: f- Annual ([PO4]_A), j- June–July–August ([PO4]_JJA), n- January–February–March ([PO4]_JFM). The sea-surface concentration of nitrates ([NO3]) in µmol/L: g- Annual ([NO3]_A), k- June–July–August ([NO3]_JJA), o- January–February –March ([NO3]_JFM). Values were downloaded from the World Ocean Atlas 2013 (Boyer et al., 2013).

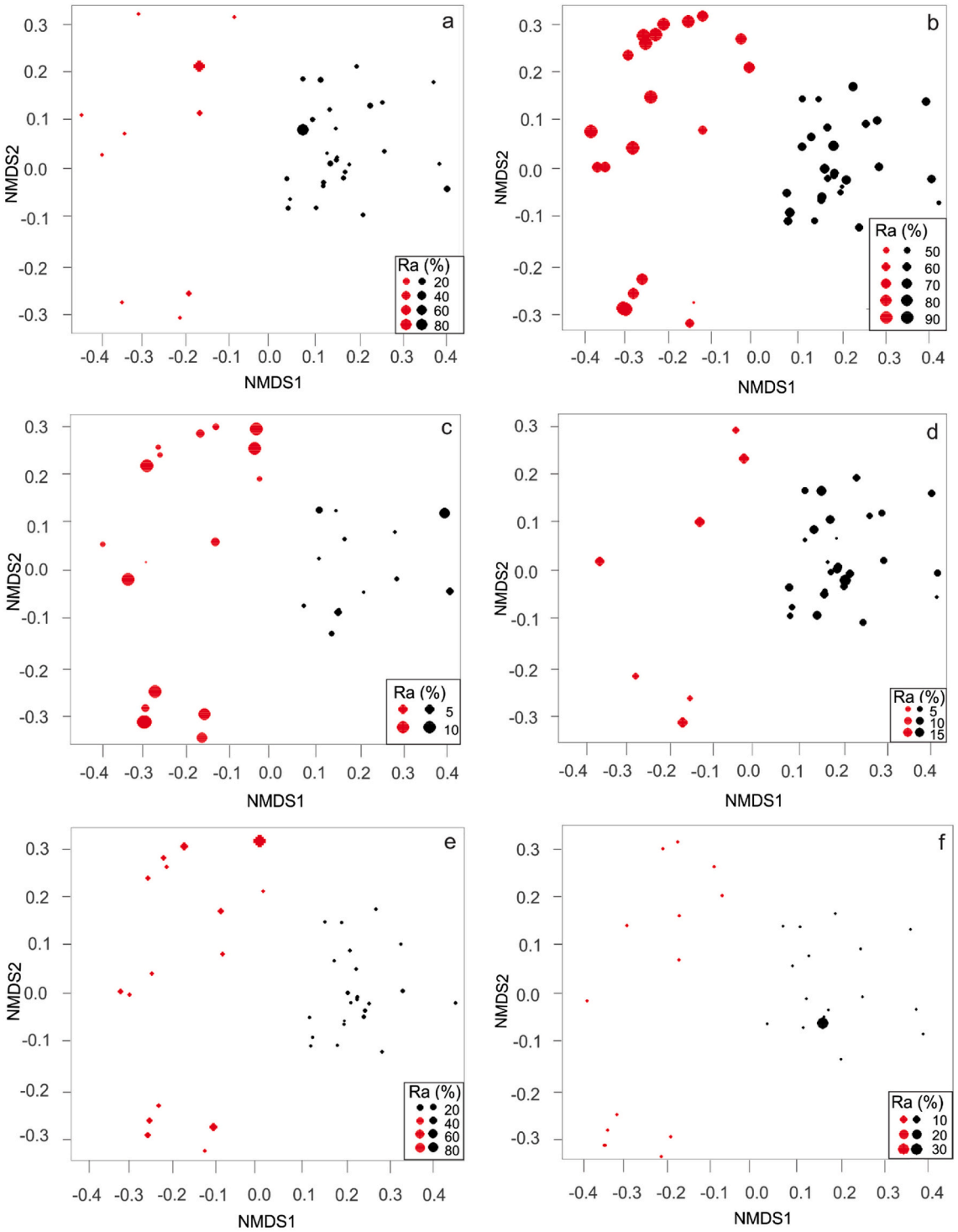

Fig. 16. Bubble plot of relative abundances (Ra %) overlaying the NMDS plot of the environmental parameters (Fig. 8a) for the Southern Caribbean (SC) (red dots) and the eastern tropical Pacific (ETP) (black dots) of: a- *Bitectatodinium spongium* b- *Brigantedinium* spp., c- cysts of *Protoceratium reticulatum*, d- *Echinidinium aculeatum*, e- *Selenopemphix nephroides* and f- *Spiniferites* spp.

abundances (less than 20% per sample) except for Zapsurro and VM12–110 from the SC where *S. nephroides* was found in relative abundances of up to (24% and 86% respectively).

The highest relative abundances of *S. nephroides* in the region occurred in shallow waters. In this environment, the cyst represents 4% of the dinocyst assemblage. In the RDA, the relative abundance of this dinocyst seems to be related to WD and DC. *S. nephroides* was observed in sediments deposited over a wide range of water depths (mean of =1324 ± 1512 m, min = 1 m, max = 5040 m) and occurs in waters influenced by coastal upwelling in the California Basin, Mexico, and Peru (Lewis et al., 1990; Vásquez-Bedoya et al., 2008; Limoges et al., 2010, 2013; Bringué et al., 2013). In the study area, the highest abundances of *S. nephroides* are reached in areas where the annual SST is higher than 27 °C and the annual SSS is between 34 and 36 psu.

On a global scale, the highest abundances of *S. nephroides* have been found in warm and high-productivity environments. The species is

classified as neritic with a strong affinity to low SSS values (Marret, 1994; Pospelova et al., 2008; Elshanawany et al., 2010; Candel et al., 2012; Zonneveld et al., 2013; Mudie et al., 2017). In Holocene sediments from the Cariaco Basin, the highest abundances of *S. nephroides* (ca. 5%) were associated with stronger trade winds and active upwelling zones during Heinrich-Stadials (González et al., 2008; Mertens et al., 2009).

5.6. *Spiniferites spp.* *Figs. 15, 16f; Plate II, 7–9*

Distribution: *Spiniferites* spp. was a common cyst in both the SC and ETP and represented 2% of the assemblages from both areas. The greatest cyst abundances were found to be associated with the highest SSS. *Spiniferites* spp. were observed in sediments deposited over a wide range of water depths (mean of =1475 ± 1591 m, min = 4 m, max = 4674 m), and the highest abundances were found at annual temperatures of >26 °C and an SSS of between 34 and 36 psu.

On a global scale, the highest abundances of *Spiniferites* spp. have been found in waters with high SST values, weak upwelling zones, and fully marine conditions (Alves de Souza et al., 2008; Holzwarth et al., 2010; Candel et al., 2012; Bringué et al., 2013; Zonneveld et al., 2013). *Spiniferites* spp. is one of the most abundant species reported in the Holocene of the Cariaco Basin and Gulf of Mexico (González et al., 2008; Mertens et al., 2009; Limoges et al., 2014).

6. Conclusions

The study of fifty-two sediment samples from the SC and the ETP reveals that of the twenty taxa recorded, six taxa (*Brigantedinium* species, *Bitectatodinium spongium, Echinidinium aculeatum*, *Selenopemphix nephroides,* cysts of *Protoceratium reticulatum,* and some *Spiniferites* spp.) dominate the cyst assemblages from these basins. *Bitectatodinium spongium*, *E. aculeatum*, and *E. granulatum* are more abundant in the ETP, while the cysts of *P. reticulatum* and *Spiniferites* spp. –both autotrophic cysts– are predominant in the SC. A lower absolute abundance of cysts was found in the SC than the ETP. This pattern is explained either by the coarser grain size of the substrate in the SC compared to the ETP, the higher primary productivity in the ETP than in the SC, and/or the lower accumulation rate of sediments that characterizes the SC compared to the ETP. NMDS and RDA analyses reveal that the relative abundance, composition, and distribution of dinocysts in the SC and the ETP are better explained by the variation of phosphates ([PO_4] Annual), seasonal nitrates ([NO_3] JJA), and seasonal SSS (JJA, and JFM). A higher Shannon Index for the ETP is consistent with a larger environmental heterogeneity, and a lower dominance of *Brigantedinium* spp. Our results provide a modern regional scale baseline for ecological, biodiversity, and paleoceanographic reconstructions in the region.

Declaration of Competing Interest

The authors declare that they have no known competing financial interests or personal relationships that could have appeared to influence the work reported in this paper.

Acknowledgements

This project was undertaken using research grants provided by COLCIENCIAS (project 1204–569–34184) and Universidad de Los Andes (Proyecto semilla VR, Programa de Investigación 2020, CG-A.). JS acknowledges financial support from COLCIENCIAS and the Vicerrectoría de Investigaciones at Universidad de Los Andes under the postdoctoral program “Es Tiempo de Volver.” MP-R acknowledges financial support from COLCIENCIAS and the University of Houston at different stages of this project. The Instituto Colombiano del Petróleo (ICP), Laboratorio Biología Marina (BIOMAR) Uniandes, the Lamont–Doherty Earth Observatory (LDEO), the Ocean Drilling Program (ODP, IODP), and EAFIT provided samples for this study. We are grateful to Professor Martin J. Head (Brock University), the handling editor Dr. Xavier Crosta, and two anonymous reviewers for valuable comments that helped to improve the quality of this article. We thank the Micropaleontology Group of M. Kucera in MARUM at Bremen University; in particular, Karin Zonneveld, for her generous support in the taxonomic determination of dinocysts. We dedicate this work to the beloved memory of our colleague and friend José Ignacio Martínez.

References

Allan, E., de Vernal, A., Krawczyk, D., Moros, M., Radi, T., Rochon, A., Seidenkrantz, M. S., Zaragosi, S., 2020. Distribution of dinocyst assemblages in surface sediment samples from the West Greenland margin. Mar. Micropaleontol. 159, 101818.

Alves de Souza, C., Varela, D., Navarrete, F., Fernandez, P., Leal, P., 2008. Distribution, abundance and diversity of modern dinoflagellate cyst assemblages from southern Chile (43–54° S). Bot. Mar. 51, 399–410.

Boyer, T.P., Antonov, J.I., Baranova, O.K., Coleman, C., Garcia, H.E., Grodsky, A., Johnson, D.R., Locarnini, R.A., Mishonov, A.V., O'Brien, T.D., 2013. NOAA Atlas NESDIS 72.

Bravo, I., Figueroa, R., 2014. Towards an ecological understanding of dinoflagellate cyst functions. Microorganisms 2, 11–32.

Bringué, M., Pospelova, V., Pak, D., 2013. Seasonal production of organic-walled dinoflagellate cysts in an upwelling system: a sediment trap study from the Santa Barbara Basin, California. Mar. Micropaleontol. 100, 34–51.

Bringué, M., Pospelova, V., Tappa, E.J., Thunell, R.C., 2019. Dinoflagellate cyst production in the Cariaco Basin: a 12.5 year-long sediment trap study. Prog. Oceanogr. 171, 175–211.

Cabarcos, E., Flores, J.A., Sierro, F.J., 2014. High-resolution productivity record and reconstruction of ENSO dynamics during the Holocene in the Eastern Equatorial Pacific using coccolithophores. The Holocene 24, 176–187.

Candel, M.S., Radi, T., de Vernal, A., Bujalesky, G., 2012. Distribution of dinoflagellate cysts and other aquatic palynomorphs in surface sediments from the Beagle Channel, Southern Argentina. Mar. Micropaleontol. 96, 1–12.

Crouch, E.M., Mildenhall, D.C., Neil, H.L., 2010. Distribution of organic-walled marine and terrestrial palynomorphs in surface sediments, offshore eastern New Zealand. Mar. Geol. 270, 235–256.

Dale, B., 1983. Dinoflagellate resting cysts. In: Frixell, G.A. (Ed.), Survival Strategies of the Algae. Cambridge University Press, New York, NY, USA, pp. 67–136.

Dale, B., 2001. Marine dinoflagellate cysts as indicators of eutrophication and industrial pollution: a discussion. Sci. Total Environ. 264, 235–240.

de Vernal, A., Rochon, A., Turon, J.L., Matthiessen, J., 1997. Organic walled dinoflagellate cysts: palynological tracers of sea-surface conditions in middle to high latitude marine environments. G'eobios 30, 905–920.

de Vernal, A., Henry, M., Bilodeau, G., 1999. Techniques de préparation et d'analyse en micropaléontologie. Les Cahiers Du GEOTOP 3, 41.

de Vernal, A., Henry, M., Matthiessen, J., Mudie, P.J., Rochon, A., Boessenkool, K.P., Eynaud, F., Grøsfjeld, K., Guiot, J., Hamel, D., Harland, R., Head, M.J., Kunz-Pirrung, M., Levac, E., Loucheur, V., Peyron, O., Pospelova, V., Radi, T., Turon, J.L., Voronina, E., 2001. Dinoflagellate cyst assemblages as tracers of sea–surface conditions in the northern North Atlantic, Arctic and sub-Arctic seas: the new 'n = 677' data base and its application for quantitative palaeoceanographic reconstruction. J. Quaternary Sci. 16, 681–698.

de Vernal, A., Radi, T., Zaragosi, S., et al., 2020. Distribution of common modern dinoflagellate cyst taxa in surface sediments of the Northern Hemisphere in relation to environmental parameters: the new n=1968 database. Mar. Micropaleontol. 159, 101796.

Durán-Quesada, A., Reboita, M., Gimeno, L., 2012. Precipitation in tropical America and the associated sources of moisture: a short review. Hydrol. Sci. J. 57, 612–624.

Elshanawany, R., Zonneveld, K., Ibrahim, M.I., Kholeif, S.E., 2010. Distribution patterns of recent organic-walled dinoflagellate cysts in relation to environmental parameters in the Mediterranean Sea. Palynology 34, 233–260.

Esper, O., Zonneveld, K.A.F., 2002. Distribution of organic-walled dinoflagellate cysts in surface sediments of the Southern Ocean (eastern Atlantic sector) between the Subtropical Front and the Weddell Gyre. Mar. Micropaleontol. 46, 177–208.

Evitt, W.R., 1985. Sporopollenin dinoflagellate cysts, their morphology and interpretation. American Association of Stratigraphic Palynologists Foundation, Dallas, Texas, U.S.A (333 p).

Fiedler, P.C., Talley, L.D., 2006. Hydrography of the eastern tropical Pacific: a review. Prog. Oceanogr. 69, 143–180.

Figueroa, R.I., Bravo, I., Garcés, E., 2008. The significance of sexual v. asexual cyst formation in the life cycle of the noxious dinoflagellate Alexandrium peruvianum. Harmful Algae 7, 653–663.

Gaines, G., Elbraechter, M., 1987. Heterotrophic nutrition. In: Taylor, F.J.R. (Ed.), The Biology of Dinoflagellates. Blackwell Scientific, Oxford, pp. 224–281.

Gardner, J.V., 1982. High-resolution carbonate and organic-carbon stratigraphies for the Late Neogene and Quaternary from the Western Caribbean and Eastern Equatorial Pacific. In: Prell, W.L., Gardner, J.V., et al. (Eds.), Init. Repts. DSDP, 68. U.S. Govt. Printing Office, Washington, pp. 347–364.

González, C., Dupont, L.M., Mertens, K., Wefer, G., 2008. Reconstructing marine productivity of the Cariaco Basin during marine isotope stages 3 and 4 using organic-walled dinoflagellate cysts. Paleoceanography 23, PA3215.

Guidi, L., Chaffron, S., Bittner, L., Eveillard, D., Larhlimi, A., Roux, S., Darzi, Y., Audic, S., Berline, L., Brum, J., Coelho, L.P., Espinoza, J.C., Malviya, S.,

Sunagawa, S., Dimier, C., Kandels-Lewis, S., Picheral, M., Poulain, J., Searson, S., Gorsky, G., 2016. Plankton networks driving carbon export in the oligotrophic ocean. Nature. 532 https://doi.org/10.1038/nature16942.
Hardy, W., Penaud, A., Marret, F., Bayon, G., Marsset, T., Droz, L., 2016. Dinocyst assemblage constrains on oceanographic and atmospheric process in the Eastern Equatorial Atlantic over the last 44 Ka. Biogeosci. Discuss. https://doi.org/10.5194/bg-2016–148.
Harland, R., 1983. Distribution maps of recent dinoflagellate cysts in bottom sediments from the North–Atlantic Ocean and adjacent seas. Palaeontology 26, 321–387.
Haug, G.H., Tiedemann, R., 1998. Effect of the formation of the Isthmus of Panama on Atlantic Ocean thermohaline circulation. Nature 393, 673–676.
Head, M., 1996. Chapter 30. Modern dinoflagellate cysts and their biological affinities. In: Jansonious, J., McGregor, D.C. (Eds.), Palynology: Principles and Applications; American Association of Stratigraphic Palynologyst Foundation, vol. 3, pp. 1197–1248.
Head, M., 2002. *Echinidinium zonneveldiae* sp. nov., a dinoflagellate cyst from the late Pleistocene of the Baltic Sea, northern Europe. J. Micropaleontol. 21, 169–173.
Hernandez-Guerra, A., Joyce, T.M., 2000. Water masses and circulation in the surface layers of the Caribbean at 661W. Geophys. Res. Lett. 27, 3497–3500.
Hidalgo, H.G., Durán-Quesada, A.M., Amador, J.A., Alfaro, E.J., 2015. The Caribbean low-level jet, the inter-tropical convergence zone and precipitation patterns in the intra-Americas sea: a proposed dynamical mechanism. Geografiska Annaler: Series A, Physical Geography 97, 41–59.
Holzwarth, U., Meggers, H., Esper, O., Kuhlmann, H., Freudenthal, T., Hensen, C., Zonneveld, K.A., 2010. NW African climate variations during the last 47,000 years: evidence from organic-walled dinoflagellate cysts. Palaeogeogr., Palaeoclimatol. Palaeoecol. 291, 443–455.
Hu, C., Montgomery, E.T., Schmitt, R.W., Muller-Karger, F.E., 2004. The dispersal of the Amazon and Orinoco River water in the tropical Atlantic and Caribbean Sea: Observation from space and S-PALACE floats. Deep-Sea Res. II Top. Stud. Oceanogr. 51, 1151–1171.
Huguet, C., Kim, J.-H., González-Arango, C., Ramírez-Valencia, V., Kang, S., Gal, J.-K., Shin, K.-H., 2019. Sources of organic matter in two contrasting tropical coastal environments: the Caribbean Sea and the eastern Pacific. J. S. Am. Earth Sci. 96, 102349.
Kameo, K., Bralower, T.J., 2000. Neogene calcareous nannofossil biostratigraphy of sites 998, 999, AND 1000, Caribbean Sea. In: Leckie, R.M., Sigurdsson, H., Acton, G.D., Draper, G. (Eds.), 2000 Proceedings of the Ocean Drilling Program, Scientific Results, 165, pp. 3–17.
Kemp, A.E.S., Mayer, L.A., Palmer-Julson, A., 1995. Neogene and Quaternary pelagic sediments and depositional history of the Eastern Ecuatorial Pacific Ocean. In: Pisias, N.G., Janecek, T.R., van Andel, T.H. (Eds.), Proceedings of the Ocean Drilling Program, Scientific Results, 138, pp. 627–639.
Kent, D., Spariosu, D., 1982. Magnetostratigraphy of Caribbean Site 502 hydraulic piston cores, 68, pp. 419–433. https://doi.org/10.2973/dsdp.proc.68.116.1982.
Kienast, S.S., Kienast, M., Mix, A.C., Calvert, S.E., Francois, R., 2007. Thorium-230 normalized particle flux and sediment focusing in the Panama Basin region during the last 30,000 years. Paleoceanography 22, PA2213.
Lea, D.W., Pak, D.-K., Spero, H.J., 2000. Climate Impact of late Quaternary Equatorial Pacific Sea Surface Temperature Variations. Science 289, 1719.
Legendre, P., Gallagher, E.D., 2001. Ecologically meaningful transformations for ordination of species data. Oecologia 129, 271–280.
Lewis, J., Dodge, D., Powell, A.J., 1990. Quaternary dinoflagellate cysts from the upwelling system offshore Peru, hole 686, ODP Leg 112. Chapter 18. In: Proc. Ocean Drill. Program. Sci. Results, 112, pp. 323–328.
Limoges, A., Kielt, J., Radi, T., Ruíz-Fernandez, A.C., de Vernal, A., 2010. Dinoflagellate cyst distribution in surface sediments along the south–western Mexican coast (14.76 N to 24.75 N). Mar. Micropaleontol. 76, 104–123.
Limoges, A., Londeix, L., de Vernal, A., 2013. Organic-walled dinoflagellate cyst distribution in the Gulf of Mexico. Mar. Micropaleontol. 102, 51–68.
Limoges, A., de Vernal, A., Van Nieuwenhove, N., 2014. Long-term hydrological changes in the northeastern Gulf of Mexico (ODP-625B) during the Holocene and late Pleistocene inferred from organic–walled dinoflagellate cysts. Paleogeography, Paleoclimatology, Paleoecology 414, 178–191.
Limoges, A., Ribeiro, S., Weckstrom, K., Heikkila, M., Zamelczyk, K., Andersen, T.J., Tallberg, P., Masse, G., Rysgaard, S., Norgaard-Pedersen, N., Seidenkrantz, M.S., 2018. Linking the modern distribution of biogenic proxies in high Arctic Greenland shelf sediments to sea ice, primary production, and Arctic-Atlantic pnflow. J Geophys Res–Biogeo 123, 760–786.
Longhurst, A., Sathyendranath, S., Platt, T., Caverhill, 1995. An estimate of global primary production in the ocean from satellite radiometer data. J. Plankton Res. 17, 1245–1271.
Maher Jr., L.J., 1981. Statistics for microfossil concentration measurements employing samples spiked with marker grains. Rev. Palaeobot. Palynol. 32, 153–191.
Marret, F., 1994. Distribution of dinoflagellate cysts in recent marine sediments from the east Equatorial Atlantic (Gulf of Guinea). Rev. Palaeobot. Palynol. 84, 1–22.
Marret, F., Zonneveld, K.A., 2003. Atlas of modern organic-walled dinoflagellate cyst distribution. Rev. Palaeobot. Palynol. 125, 1–200.
Marret, F., De Vernal, A., Benderra, F., Harland, R., 2001. Late Quaternary Sea-surface conditions at DSDP Hole 594 in the Southwest Pacific Ocean based on dinoflagellate cyst assemblages. J. Quat. Sci. 16, 739–751.
Marret, F., Bradley, L., de Vernal, A., et al., 2020. From bi-polar to regional distribution of modern dinoflagellate cysts, an overview of their biogeography. Mar. Micropaleontol. 159, 101753.
Matthiessen, J., de Vernal, A., Head, M., et al., 2005. Modem organic-walled dinoflagellate cysts in arctic marine environments and their (paleo-) environmental significance. Paläontol. Z. 79, 3–51.
McCartney, K., Churchill, S., Woestendiek, L., 1995. Silicoflagellates and ebridians from LEG 138, Eastern Equatorial Pacific. In: Pisias, N.G., Mayer, L.A., Janecek, T.R., Palmer-Julson, A., van Andel, T.H. (Eds.), 1995 Proceedings of the Ocean Drilling Program, Scientific Results, vol. 138, pp. 129–162.
Mertens, K.N., González, C., Delusina, I., Louwye, S., 2009. 30 000 years of productivity and salinity variations in the late Quaternary Cariaco Basin revealed by dinoflagellate cysts. Boreas 38, 647–662.
Mertens, K.N., Dale, B., Ellegaard, M., Jansson, I.-M., Godhe, A., Kremp, A., Louwye, S., 2011. Process length variation in cysts of the dinoflagellate *Protoceratium reticulatum*, from surface sediments of the Baltic-Kattegat-Skagerrak estuarine system: a regional salinity proxy. Boreas 40, 242–255.
Mertens, K.N., Carbonell-Moore, M.C., Pospelova, V., Head, M.J., Highfield, A., Schroeder, D., et al., 2018. *Pentaplacodinium saltonense* gen. Et sp. nov. (Dinophyceae) and its relationship to the cyst-defined genus *Operculodinium* and yessotoxin-producing *Protoceratium reticulatum*. Harmful Algae 71, 57–77.
Milliman, J.D., 1990. Fluvial sediment in coastal seas: flux and fate. Nature and Resources (Unesco) 26, 12–22.
Montes, C., Cardona, A., Jaramillo, C., Pardo, A., Valencia, V., Ayala, C., Perez-Angel, L. C., Rodriguez-Parra, L.A., Ramirez, V., Nino, H., 2015. Middle Miocene closure of the central American Seaway. Science 348, 226–229.
Montresor, M., Lovejoy, C., Orsini, L., Procaccini, G., Roy, S., 2003. Bipolar distribution of the cyst-forming dinoflagellate *Polarella glacialis*. Polar Bio. 26, 186–194.
Mora, A., Parra, M., Strecker, M., Kammer, A., Dimaté, C., Rodríguez, F., 2006. Cenozoic contractional reactivation of Mesozoic extensional structures in the Eastern Cordillera of Colombia. Tectonics 25, TC2010.
Mora, A., Moreau, C., Moquet, J.S., Gallay, M., Mahlknecht, J., Laraque, A., 2020. Hydrological control, fractionation, and fluxes of dissolved rare earth elements in the lower Orinoco River, Venezuela. Appl. Geochem. 112, 104462.
Mudie, P.J., 1992. Circum-arctic Quaternary and Neogene marine palynofloras: Paleoecology and statistical analysis. In: Head, M.J., Wrenn, J.H. (Eds.), Neogene and Quaternary Dinoflagellate Cysts and Acritarchs. American Association of Stratigraphic Palynologists Foundation, Dallas, pp. 347–390.
Mudie, P.J., Marret, F., Mertens, K.N., Shumilovskikh, L., Leroy, S.A., 2017. Atlas of modern dinoflagellate cyst distributions in the Black Sea Corridor: from Aegean to Aral Seas, including Marmara, Black, Azov and Caspian Seas. Mar. Micropaleontol. 134, 1–152.
Müller-Karger, F., Varela, R., Thunell, R., Astor, Y., Zhang, H., Luerssen, R., Hu, C., 2004. Processes of coastal upwelling and carbon flux in the Cariaco Basin. Deep-Sea Res. II Top. Stud. Oceanogr. 51, 927–943.
Narale, D., Jagadish, P., Arga, A., 2013. Dinoflagellate cyst distribution in recent sediments along the south-east coast of India. Oceanologia 55, 979–1003.
O'Dea, A., Lessios, H.A., Coates, A.G., Eytan, R.I., Restrepo-Moreno, S.A., Cione, A.L., Collins, L.S., de Queiroz, A.D., Farris, W.R., Norris, D., et al., 2016. Formation of the Isthmus of Panama. Sci. Adv. 2, 1–11.
Oksanen, J., Blanchet, F.G., Kindt, R., Legendre, P., O'hara, R., Simpson, G.L., Solymos, 2014. Vegan: Community Ecology Package. R Package Version 2, 2. http://CRAN.Rproject.org/package=vegan.
Orlova, T.Y., Morozova, T.V., Gribble, K.E., Kulis, D.M., Anderson, D.M., 2004. Dinoflagellate cysts in recent marine sediments from the east coast of Russia. Bot. Mar. 47, 185–201.
Paez-Reyes, M., Head, M.J., 2013. The Cenozoic Gonyaulacacean Dinoflagellate Genera *Operculodinium* Wall, 1967 and *Protoceratium* Bergh, 1881 and their Phylogenetic Relationships Cenozoic Gonyaulacacean Dinoflagellates. J. Paleontol. 87, 786–803.
Peterson, L.C., Haug, G.H., Murray, R.W., Yarincik, K.M., King, J.W., Bralower, T.J., Kameo, K., Rutherford, S.D., Pearce, R.B., 2000. Late Quaternary stratigraphy and sedimentation at site 1002, Cariaco Basin (Venezuela). In: Leckie, R.M., Sigurdsson, H., Acton, G.D., Draper, G. (Eds.), Proceedings of the Ocean Drilling Program, Scientific Results, 165, pp. 85–99.
Pospelova, V., Kim, S., 2010. Dinoflagellate cysts in recent estuarine sediments from aquaculture sites of southern South Korea. Mar. Micropaleontol. 76, 37–51.
Pospelova, V., de Vernal, A., Pedersen, T.F., 2008. Distribution of dinoflagellate cysts in surface sediments from the northeastern Pacific Ocean (43–25°N) in relation to sea surface temperature, salinity, productivity and coastal upwelling. Mar. Micropaleontol. 68, 21–48.
Poveda, G., Mesa, O.J., 1997. Feedbacks between hydrological processes in tropical South America and large-scale ocean atmospheric phenomena. J. Clim. 10, 2690–2702.
Poveda, G., Waylen, P.R., Pulwarty, R.S., 2006. Annual and inter-annual variability of the present climate in northern South America and southern Mesoamerica. Palaeogeogr. Palaeoclimatol. Palaeoecol. 234, 3–27.
Poveda, G., Jaramillo, L., Vallejo, L.F., 2014. Seasonal precipitation patterns along pathways of South American low-level jets and aerial rivers. Water Resour. Res. 50, 98–118.
Prebble, J.G., Crouch, E.M., Carter, L., Cortese, G., Bostock, H., Neil, H., 2013. An expanded modern dinoflagellate cyst dataset for the Southwest Pacific and Southern Hemisphere with environmental associations. Mar. Micropaleontol. 101, 33–48.
Price, A.M., Pospelova, V., Coffin, M.R.S., Latimer, J.S., Chmura, G.L., 2016. Biogeography of dinoflagellate cysts in Northwest Atlantic estuaries. Ecology and Evolution 6, 5648–5662.
QGIS Development Team, 2014. QGIS Geographic Information System. Open Source Geospatial Foundation Project. http://qgis.osgeo.org.
R core Team, 2015. R: A language and environment for statistical computing.

Radi, T., de Vernal, A., 2004. Dinocyst distribution in surface sediments from the northeastern Pacific margin (40–60° N) in relation to hydrographic conditions, productivity and upwelling. Rev. Palaeobot. Palynol. 128, 169–193.
Restrepo, J., Kjerfve, B., 2004. The Pacific and Caribbean Rivers of Colombia: Water Discharge, Sediment Transport and Dissolved Loads. In: Heidelberg, S. (Ed.), Environmental Geochemistry in Tropical and Subtropical Environments. Springer, pp. 169–187.
Restrepo, J.D., López, S.A., 2008. Morphodynamics of the Pacific and Caribbean deltas of Colombia, South America. J. S. Am. Earth Sci. 25, 1–21.
Ribeiro, S., Amorim, A., 2008. Environmental drivers of temporal succession in recent dinoflagellate cyst assemblages from a coastal site in the North–East Atlantic (Lisbon Bay, Portugal). Mar. Micropaleontol. 68, 156–178.
Rincón-Martínez, D., Lamy, F., Contreras, S., Leduc, G., Bard, E., Saukel, C., Blanz, T., Mackensen Tiedemann, R., 2010. More humid interglacials in Ecuador during the past 500 kyr linked to latitudinal shifts of the equatorial front and the Intertropical Convergence Zone in the eastern tropical Pacific. Paleoceanography 25, PA2210.
Rochon, A., Vernal, A.d., Turon, J., Matthießen, J., Head, M.J., 1999. Distribution of recent dinoflagellate cysts in surface sediments from the North Atlantic Ocean and adjacent seas in relation to sea-surface parameters. American Association of Stratigraphic Palynologists Contribution Series 35, 1–146.
Sangiorgi, F., Donders, T.H., 2004. Reconstructing 150 years of eutrophication in the North-Western Adriatic Sea (Italy) using dinoflagellate cysts, pollen and spores. Estuar. Coast. Shelf Sci. 60, 69–79.
Schlitzer, R., 2017. Ocean Data View. http://odv.awi.de.
Schnepf, E., Elbrächter, M., 1992. Nutritional strategies in dinoflagellates. A review with emphasis on cell biological aspects. European Journal of Protistology. 28, 3–24.
Stockmarr, J., 1971. Tabletes with spores used in absolute pollen analysis. Pollen Spores 13, 615–621.
Sluijs, A., Brinkhuis, H., Crouch, E.M., John, C.M., Handley, L., Munsterman, D., Dickens, G.R., 2008. Eustatic variations during the Paleocene-Eocene greenhouse world. Paleoceanography 23 (4).
Sullivan, K., 1992. Late Quaternary Periplatform Sediments and Environments on the Northeastern Nicaragua Rise, Caribbean Sea. Ph. D Thesis. Rice University, Houston, Texas (244 p).
Taylor, F., Hoppenrath, M., Saldarriaga, J.F., 2008. Dinoflagellate diversity and distribution. Biodivers. Conserv. 17, 407–418.
Van Nieuwenhove, N., Head, M.J., Limoges, A., Pospelova, V., Metens, K.N., Matthiessen, J., et al., 2020. An overview and brief description of common marine organic-walled dinoflagellate cyst taxa occurring in surface sediments of the Northern Hemisphere. Mar. Micropaleontol. 159, 101814.
Vásquez-Bedoya, L., Radi, T., Ruiz-Fernández, A., De Vernal, A., Machain-Castillo, M., Kielt, J., Hillaire-Marcel, C., 2008. Organic-walled dinoflagellate cysts and benthic foraminifera in coastal sediments of the last century from the Gulf of Tehuantepec, South Pacific Coast of Mexico. Mar. Micropaleontol. 68, 49–65.
Verleye, T.J., Louwye, S., 2010. Recent geographical distribution of organic-walled dinoflagellate cysts in the Southeast Pacific (25-53 S) and their relation to the prevailing hydrographical conditions. Palaeogeogr., Palaeoclimatol. Palaeoecol. 298, 319–340.
Verleye, T.J., Mertens, K.N., Young, M.D., Dale, B., McMinn, A., Scott, L., et al., 2012. Average process length variation of the marine dinoflagellate cyst *Operculodinium centrocarpum* in the tropical and Southern Hemisphere Oceans: Assessing its potential as a palaeosalinity proxy. Mar. Micropaleontol. 86-87, 45–58.
Vink, A., Zonneveld, K.A., Willems, H., 2000. Organic–walled dinoflagellate cysts in western equatorial Atlantic surface sediments: distributions and their relation to environment. Rev. Palaeobot. Palynol. 112, 247–286.
Wall, D., 1965. Modern hystrichospheres and dinoflagellate cysts from the Woods Hole region. Grana Palynologica 6, 297–314.
Wall, D., Dale, B., 1966. "Living fossils" in western Atlantic plankton. Nature 211, 1025–1026.
Wall, D., Dale, B., 1968. Modern dinoflagellate cysts and evolution of the Peridiniales. Micropaleontology 14, 265–304.
Wall, D., Dale, B., Lohmann, G., Smith, W.K., 1977. The environmental and climatic distribution of dinoflagellate cysts in modern marine sediments from regions in the North and South Atlantic Oceans and adjacent seas. Mar. Micropaleontol. 2, 121–200.
Wang, C., 2007. Variability of the Caribbean low–level jet and its relations to climate. Clim. Dyn. 29, 411–422.
Wang, N., Mertens, K.N., Krock, B., Luo, Z., Derrien, A., Pospelova, V., et al., 2019. Cryptic speciation in *Protoceratium reticulatum* (Dinophyceae): evidence from morphological, molecular and ecophysiological data. Harmful Algae 88, 101610.
Williams, G.L., Fensome, R.A., MacRae, R.A., 2017. The Lentin and Williams Index of fossil dinoflagellates. American Association of Stratigraphic Palynologists, AASP Contribution Series 48 (1097 p).
Wood, G.D., Gabriel, A.M., Lawson, J.C., 1996. Palynological techniques-processing and microscopy. In: Jansonius, J., McGregor, D.C. (Eds.), Palynology: Principles and Applications, vol. 1. American Association of Stratigraphic Palynologists Foundation, Dallas, TX, pp. 29–50.
Zonneveld, K.A.F., 1997. New species of organic walled dinoflagellate cysts from modern sediments of the Arabian Sea (Indian Ocean). Rev. Palaeobot. Palynol. 97, 319–337.
Zonneveld, K.A.F., Jurkschat, T., 1999. *Bitectatodinium spongium* (Zonneveld, 1997) Zonneveld et Jurkschat, comb. nov. from modern sediments and sediment trap samples of the Arabian Sea (northwestern Indian Ocean): taxonomy and ecological affinity. Rev. Palaeobot. Palynol. 106, 153–169.
Zonneveld, K.A.F., Pospelova, V., 2015. A determination key for modern dinoflagellate cysts. Palynology. 39, 387–407.
Zonneveld, K.A.F., Bockelmann, F., Holzwarth, U., 2007. Selective aerobic degradation of organic-walled dinoflagellates as tool to quantify past net primary production and bottom water oxygen concentrations. Mar. Geol. 237, 109–126.
Zonneveld, K.A.F., Susek, E., Fischer, G., 2010. Seasonal variability of the organic-walled dinoflagellate cyst production in the coastal upwelling region off Cape Blanc (Mauritania): a five-year survey. J. Phycol. 46, 202–215.
Zonneveld, K.A.F., Marret, F., Versteegh, G.J.M., Bogus, K., Bonnet, et al., 2013. Atlas of modern dinoflagellate cyst distribution based on 2405 data points. Rev. Palaeobot. Palynol. 191, 1–197.